Production and decay of scalar top squarkonium bound states

Manuel Drees

Physics Department, University of Wisconsin, Madison, Wisconsin 53706

Mihoko M. Nojiri*

Theory Group, KEK, Oho 1-1, Tsukuba, Ibaraki 305, Japan

(Received 6 December 1993)

In this paper we discuss possible signatures for the production of scalar $\tilde{t}_1 \tilde{t}_1^*$ (top squarkonium) bound states $\sigma_{\tilde{t}_1}$ at hadron colliders, where $\tilde{t}_1$ is the lighter scalar top eigenstate. We first study the decay of $\sigma_{\tilde{t}_1}$; explicit expressions are given for all potentially important decay modes. If $\tilde{t}_1$ has unsuppressed two-body decays, they will always overwhelm the annihilation decays of $\sigma_{\tilde{t}_1}$. Among the latter, we find that usually either the gg or hh final state dominates, depending on the size of the off-diagonal entry of the top squark mass matrix; h is the lighter neutral scalar Higgs boson of the minimal supersymmetric model. If $m_{\sigma_{\tilde{t}}}$ happens to be close to the mass of one of the neutral scalar Higgs bosons, $Q\bar{Q}$ final states dominate ($Q = b$ or t). $W^+ W^-$ and ZZ final states are subdominant. We argue that $\sigma_{\tilde{t}_1} \to \gamma\gamma$ decays offer the best signal for top squarkonium production at hadron colliders. The Fermilab Tevatron should be able to close the light top squark window left open by CERN LEP searches, but its mass reach is limited to $m_{\sigma_{\tilde{t}}} \lesssim 90$ GeV. In contrast, at the CERN LHC one should ultimately be able to probe the region $m_{\sigma_{\tilde{t}}} \lesssim 700$ GeV, if the hh partial width is not too large. We also comment on the feasibility of searching for $\sigma_{\tilde{t}_1}$ production at hadron colliders in the ZZ, $Z\gamma$, and $\tau^+ \tau^+ \tau^- \tau^-$ final states, and briefly mention $\sigma_{\tilde{t}_1}$ production at $\gamma\gamma$ colliders.

PACS number(s): 14.80.Ly, 12.60.Jv, 13.85.Qk

I. INTRODUCTION

Although the standard model (SM) of particle physics [1] has so far passed all experimental tests, it has long been known [2] to be technically unnatural: Nothing protects the mass of the Higgs boson, and hence the scale of electroweak symmetry breaking, from large (quadratically divergent) radiative corrections which "naturally" push it up to the Planck scale or the scale M_X of grand unified theories (GUT's). Probably the most elegant solution [3] of this problem is the introduction of $N = 1$ supersymmetry (SUSY) [4]. In supersymmetric theories corrections to the mass of the Higgs boson from loops involving SM particles are automatically canceled by loops involving their superpartners. The cancellation is not perfect since supersymmetry has to be broken; naturalness arguments then suggest that the scale of SUSY breaking should not (much) exceed 1 TeV.

So far, searches for the direct production of superparticles (sparticles) in collider experiments have not been successful. However, the lower limits on their masses that can be inferred from these searches are only around 120 GeV for most strongly interacting sparticles [5] and under 50 GeV for all other sparticles [6]. This leaves a wide region to be explored by present and future experiments, and much work in that direction has already been done [4,7].

Meanwhile, various indirect (loop) effects due to supersymmetric particles have been investigated. A by-now well-known result [8] is that the introduction of supersymmetry allows for a beautiful unification of all three gauge couplings of the SM at a scale $M_X \simeq 10^{16}$ GeV. In contrast, nonsupersymmetric theories can be unified only at the cost of the somewhat *ad hoc* introduction of new degrees of freedom and/or intermediate scales between M_X and M_W. Unfortunately, these analyses only tell us [8,9] that the scale of SUSY breaking should not exceed 10 TeV or so and hence offer no immediate clues where to look for more direct evidence for the existence of supersymmetric particles.

Such a clue might come from the third main motivation for the introduction of SUSY. In addition to technical naturalness and simple grand unification, supersymmetric theories also offer the possibility to *understand* (as opposed to parametrize) electroweak gauge symmetry breaking in terms of (logarithmic) radiative corrections to scalar masses. Even if all these masses are identical at some very high energy scale where SUSY breaking becomes effective, as, e.g., in minimal supergravity theories [4], radiative corrections will drive the square of the mass of one Higgs boson doublet to negative values at low energies, leaving all other squared scalar masses positive [10]. The driving force in this radiative symmetry breaking is the large Yukawa coupling of the top quark: Radiative corrections due to Yukawa couplings reduce scalar masses, while gauge interactions increase them. This mechanism not only establishes a causal link between the

*Electronic address: NOJIRIN@JPNKEKVX

breaking of supersymmetry and the breakdown of electroweak gauge symmetry, it also points toward a fundamental role for a large (top) Yukawa coupling and might thus eventually help to understand why the top quark is so much heavier than all other SM fermions.

In more practical terms, these considerations indicate that the superpartners of the top quark, the top squarks, might be considerably *lighter* than the other squarks [11]; recall that radiative corrections due to Yukawa interactions *reduce* scalar masses. In addition, a large Yukawa coupling implies large mass mixing between the superpartners of left- and right-handed top quarks, which further reduces the mass of the lighter top squark eigenstate $\tilde{t}_1$. As a result, even in minimal supergravity models $m_{\tilde{t}_1}$ can be almost arbitrarily light even if all other squarks have masses of several hundred GeV [12,13].

What is the experimental situation? Top squarks are color triplets and thus have substantial pair production cross sections at hadron colliders. However, present experimental bounds [5] on squark masses assume 10 or 12 degenerate squark eigenstates and therefore do not apply to $\tilde{t}_1$; at present, searches for events with large missing transverse energy cannot exclude the existence of a light top squark if the mass of the lightest supersymmetric particle (LSP) exceeds 12 GeV or so [14]. This bound is expected to improve once the data taken during the 1992–1993 collider run have been analyzed; however, the signal for open top squark production at hadron colliders will always become invisible as the top squark–LSP mass difference is reduced.

Top squarks also have electromagnetic and weak interactions. However, for a certain $\tilde{t}_L$-$\tilde{t}_R$ mixing angle θ_t the $Z\tilde{t}_1\tilde{t}_1^*$ coupling vanishes [15], so that *no* strict lower bound on $m_{\tilde{t}_1}$ can be derived from the study of Z decays. In this scenario, $\tilde{t}_1$ pair production at e^+e^- colliders can only proceed via photon exchange. The lower bound on $m_{\tilde{t}_1}$ will then again depend on the LSP mass, since for too small a $\tilde{t}_1$-LSP mass difference $\tilde{t}_1$ pair events look more and more like hadronic two-photon events.[1]

One might worry that a light top squark produces unacceptably large loop effects. Indeed, a light top squark can lead to large corrections to the electroweak ρ parameter and related quantities [21]. However, the main effect would be a reduction of the value of the top

quark mass m_t fitted from electroweak data; note that at present the central value of the SM fit of m_t [22] is substantially above the direct search limit on m_t [23]. Moreover, this search limit is only valid in the SM. If $\tilde{t}_1$ is light enough, the decay $t \rightarrow \tilde{t}_1 + LSP$ can significantly dilute the dilepton signal for the top, especially if $m_t \leq 90$ GeV [14]. In any case, a small $m_{\tilde{t}_1}$ need not imply large contributions to $\delta\rho$ [21]. Similarly, loops involving top squarks and charginos can contribute significantly to the matrix element for $b \rightarrow s\gamma$ decays [24]. However, this contribution can be canceled by other non-SM loop contributions involving charged Higgs bosons. As a result, the recent bounds [25] on the branching ratio for $b \rightarrow s\gamma$ do not exclude [18] a very light $\tilde{t}_1$.

We thus conclude that a $\tilde{t}_1$ of 40 or 50 GeV could quite easily have escaped detection so far; if we are willing to fine-tune the $Z\tilde{t}_1\tilde{t}_1^*$ coupling and the $\tilde{t}_1$-LSP mass difference even a 15 or 20 GeV $\tilde{t}_1$ is not excluded. This also indicates that it is difficult to obtain stringent bounds on $m_{\tilde{t}_1}$ from searches for open $\tilde{t}_1$ production. In particular, most signals will disappear in the limit where $\tilde{t}_1$ becomes (almost) degenerate with the LSP; unlike for, say, first-generation squarks and gluinos, this is possible even in the restrictive class of minimal supergravity models.[2]

On the other hand, if the $\tilde{t}_1$-LSP mass difference is small, $\tilde{t}_1$ will be rather long lived [27]. The reason is that in this case two-body tree-level decays such as $\tilde{t}_1 \rightarrow t + LSP$ or $\tilde{t}_1 \rightarrow b +$ chargino are kinematically forbidden. In this situation, $\tilde{t}_1$ decays preferably into a charm quark and a neutralino via a loop diagram, whose decay width is suppressed by a factor $\sim 10^{-7}$ compared to tree-level decays [27]. Being long lived, top squarks can form bound states ("top squarkonia"), which eventually decay via $\tilde{t}_1\tilde{t}_1^*$ annihilation into final states that only contain SM particles.

In this paper we study the decay of scalar (S-wave) $\tilde{t}_1\tilde{t}_1^*$ bound states $\sigma_{\tilde{t}_1}$ as well as possible signals for $\sigma_{\tilde{t}_1}$ production at hadron (super)colliders. Scalar top squarkonium has been studied previously in Refs. [28–30]. However, in Refs. [28] and [30] mixing between the superpartners of left- and right-handed top quarks was ignored, and diagrams involving Higgs bosons in the intermediate or final state were treated only in an approximate fashion or not at all; both effects can be very important. They have been included in Ref. [29], but there only a very light $\sigma_{\tilde{t}_1}$ was treated, so that many decay channels were kinematically forbidden. We computed the decay widths for all tree-level two-body decays of $\sigma_{\tilde{t}_1}$ for general top squark mixing and the whole range of masses of interest in the foreseeable future. As already pointed out in Ref. [31], the two-photon decay of $\sigma_{\tilde{t}_1}$ probably offers the best signal at hadron colliders. Here we present a more detailed discussion of the region of parameter space

---

[1]The TOPAZ Collaboration at the KEK TRISTAN collider recently observed [16] a slight excess of D^* mesons when trying to measure two-photon production of charm. This has caused speculations [17,13,18] that there might be a top squark with mass between 15 and 20 GeV; $\tilde{t}_1\tilde{t}_1^*$ production would then give a similar signal as two-photon production of charm if the LSP lies just a few GeV below the top squark. However, the QCD prediction for $\sigma(\gamma\gamma \rightarrow c\bar{c})$ is quite uncertain [19]; the measured cross section is only about 1.5 standard deviations above the upper range of QCD predictions. Moreover, preliminary data from the VENUS Collaboration [20] indicate that the $\tilde{t}_1$-LSP mass difference would have to be as small as 2.5 GeV for $\tilde{t}_1$ to have escaped detection. Interpretation of the excess in terms of a rather contrived SUSY model therefore seems premature.

[2]At least in models with exact R parity, $\tilde{t}_1$ cannot actually be the LSP, since searches for exotic isotopes imply [26] that the LSP has to be electrically and color neutral.

where this signal is viable. We also point out that an interesting range of $\sigma_{\tilde{t}_1}$ masses should already be accessible at the Fermilab Tevatron.

The rest of this article is organized as follows. In Sec. II we discuss $\sigma_{\tilde{t}_1}$ decays. Final states consisting of two gluons or two scalar Higgs bosons usually are dominant among decays that proceed by $\tilde{t}_1\tilde{t}_1^*$ annihilation. Contrary to claims in Refs. [28,30], final states containing two heavy gauge bosons contribute much less to the total width of $\sigma_{\tilde{t}_1}$; this is a direct consequence of electroweak gauge invariance. In Sec. III we discuss signals for $\sigma_{\tilde{t}_1}$ production at present and future hadron colliders. We focus on the clean two-photon signal, whose background can be calculated relatively reliably. At future supercolliders a signal consisting of four τ leptons may also be viable, but here realistic background estimates are much

more difficult. Section IV contains a summary of our main results and some conclusions. Explicit expressions for all $\sigma_{\tilde{t}_1}$ two-body decays are collected in the Appendix.

II. TOP SQUARKONIUM DECAYS

In this section we discuss the decays of scalar $\tilde{t}_1\tilde{t}_1^*$ bound states $\sigma_{\tilde{t}_1}$. We work within the framework of the minimal supersymmetric standard model (MSSM) [4], which is a supersymmetrization of the SM with minimal Higgs sector. In particular, every quark gets two superpartners described by complex scalar fields, which are associated with the left- and right-handed components of the quark Dirac spinor. If the quark is massive, its two superpartners can mix with each other. For the case of top squarks, the resulting mass matrix is given by [11] [in the basis $(\tilde{t}_L, \tilde{t}_R)$]

$$\mathcal{M}_{\tilde{t}}^2 = \begin{bmatrix} m_{\tilde{t}_L}^2 + m_t^2 + 0.35m_Z^2\cos2\beta & -m_t(A_t + \mu\cot\beta) \\ -m_t(A_t + \mu\cot\beta) & m_{\tilde{t}_R}^2 + m_t^2 + 0.16m_Z^2\cos2\beta \end{bmatrix}, \tag{1}$$

where we have used the conventions of Ref. [12], which are quite similar to those of Ref. [32]. The quantities $m_{\tilde{t}_L}, m_{\tilde{t}_R}$ describe the soft SUSY-breaking contributions to the diagonal squark masses. As already mentioned in the Introduction, loop corrections involving the top Yukawa coupling tend to reduce these mass parameters compared to their values at higher energies. In models where all squark masses are equal at some very high (GUT or Planck) scale, one therefore expects $m_{\tilde{t}_{L,R}}$ to be *smaller* than the corresponding quantities for squarks of the first two generations. The same argument also implies $m_{\tilde{t}_R} < m_{\tilde{t}_L}$, since Yukawa interactions affect the running of $m_{\tilde{t}_R}$ more strongly [10].

The diagonal entries of the stop mass matrix (1) also depend on the mass m_t of the top quark as well as the angle β, defined via $\tan\beta \equiv \langle H_2^0 \rangle / \langle H_1^0 \rangle$, where H_1, H_2 are the two Higgs doublet fields necessary in any realistic supersymmetric model [4]. Two additional parameters enter the off-diagonal entries of (1): The supersymmetric Higgs(ino) mass μ and the parameter A_t describing the strength of the trilinear scalar $H_2^0\tilde{t}_L\tilde{t}_R^*$ interaction, which breaks supersymmetry. A_t and μ are free parameters of the model, but we generally expect them to be of roughly the same magnitude as $m_{\tilde{t}_{L,R}}$; $\tan\beta$ can be taken to be positive, but both A_t and μ can have either sign.

The mass matrix (1) can easily be diagonalized. We define

$$\begin{bmatrix} \tilde{t}_1 \\ \tilde{t}_2 \end{bmatrix} = \begin{bmatrix} \cos\theta_t & \sin\theta_t \\ -\sin\theta_t & \cos\theta_t \end{bmatrix} \begin{bmatrix} \tilde{t}_L \\ \tilde{t}_R \end{bmatrix} \tag{2}$$

and obtain

$$m_{\tilde{t}_{1,2}}^2 = \tfrac{1}{2}[m_{LL}^2 + m_{RR}^2 \mp \sqrt{(m_{LL}^2 - m_{RR}^2)^2 + 4m_{LR}^4}], \tag{3a}$$

$$\tan\theta_t = \frac{m_{\tilde{t}_1}^2 - m_{LL}^2}{m_{LR}^2}, \tag{3b}$$

where $m_{LL,LR,RR}^2$ are the (1,1), (1,2), and (2,2) elements of the mass matrix (1), respectively. Note that $\cos^2\theta_t < (>) \tfrac{1}{2}$ if $m_{\tilde{t}_L}^2 > (<) m_{\tilde{t}_R}^2$.

We will see below that $\sigma_{\tilde{t}_1}$ decays can involve charginos and neutralinos as well as Higgs bosons; we therefore briefly describe the corresponding sectors of the MSSM. The charginos $\tilde{W}_1, \tilde{W}_2$ are [4] mixtures of the superpartners of the $W^\pm$ bosons and of the charged Higgs fields contained in $H_{1,2}$. Similarly, the neutralinos $\tilde{Z}_i$, $i = 1, \ldots, 4$, are mixtures of the superpartners of the (unmixed) B and W_3 gauge bosons of the SM as well as of the neutral Higgs bosons. Charginos are Dirac fields, while neutralinos can be described by Majorana spinors. The mass matrices for charginos and neutralinos depend [4] on the parameters μ and $\tan\beta$ introduced above, as well as on the SUSY-breaking gaugino masses M_1 and M_2. We will for simplicity assume the usual unification relation $M_1 = \tfrac{5}{3}\tan^2\theta_W M_2 \simeq M_2/2$; similarly, the gluino mass is given by $M_3 = \alpha_s \sin^2\theta_W M_2/\alpha$. The description of the neutralino, chargino, and gluino sectors thus only necessitates the introduction of one additional parameter, which we take to be the mass M_2 (at the weak scale). Finally, at the tree level the Higgs sector of the MSSM is described by two parameters [32], which we take to be $\tan\beta$ and the mass m_P of the pseudoscalar Higgs boson. We have included radiative corrections to the Higgs boson masses and mixings from top-quark–top-squark loops [33], employing the effective potential formalism [34]; these corrections are determined completely in terms of the parameters entering the top squark mass matrix (1).

We are now in a position to discuss $\sigma_{\tilde{t}_1}$ decays. There are two very different kinds of decay modes: *single top squark decays*, where one top squark decays independently of the second squark, and *annihilation decays*, which proceed by $\tilde{t}_1 \tilde{t}_1^*$ annihilation. The $\sigma_{\tilde{t}_1}$ partial widths due to single top squark decays are simply twice the corresponding top squark decay widths. Since we are interested in relatively light top squarks, we will assume that $\tilde{t}_1 \rightarrow t + \tilde{g}$ decays are kinematically forbidden. We then have to consider the following two-body $\tilde{t}_1$ decays:

$$\tilde{t}_1 \rightarrow b \tilde{W}_i, \quad i=1,2 , \tag{4a}$$

$$\tilde{t}_1 \rightarrow t \tilde{Z}_j, \quad j=1,\dots,4 , \tag{4b}$$

$$\tilde{t}_1 \rightarrow c \tilde{Z}_j, \quad j=1,\dots,4 . \tag{4c}$$

The processes (4a) and (4b) occur at the tree level, with full gauge or top Yukawa strength. If they are kinematically unsuppressed, the corresponding $\tilde{t}_1$ decay widths are very roughly of order $(10^{-3}-10^{-2})m_{\tilde{t}_1}$; exact expressions are listed in the Appendix [Eqs. (A16) and (A17)].

If the channels (4a) and (4b) are kinematically closed, (4c) is usually the dominant decay mode [27] of $\tilde{t}_1$. Note that it couples a third-generation squark to a second-generation quark via a neutral (super)current. In models where the squark mass matrix and the quark Yukawa coupling matrix commute at some energy scale, e.g., if all squarks are mass degenerate at some energy scale, the process (4c) therefore has to proceed via a weak loop diagram involving small elements of the quark flavor mixing matrix. Even though the amplitude is enhanced by a factor $\ln(M_X/M_W)$, the authors of Ref. [27] therefore estimate the squared matrix element for the process (4c) to be suppressed by a factor $\sim 10^{-7}$ compared to the tree-level process (4b), leading to a decay width $\sim 10^{-9}m_{\tilde{t}_1}$. We will see below that this is completely negligible compared to the widths for annihilation decays, to which we turn next.[3]

As already mentioned, these proceed via the annihilation of the $\tilde{t}_1$ and $\tilde{t}_1^*$ that make up $\sigma_{\tilde{t}_1}$; this kind of decay by far dominates the total widths of the familiar lowest-lying quarkonium states ($\eta_c, J/\psi, \Upsilon$). Here we are only interested in two-body decays of $\sigma_{\tilde{t}_1}$, which dominate all other annihilation decays. We treat $\sigma_{\tilde{t}_1}$ as a nonrelativistic bound state, where the squarks are in an S wave. The partial width for $\sigma_{\tilde{t}_1} \rightarrow A + B$ is then given by [35,36]

$$\Gamma(\sigma_{\tilde{t}_1} \rightarrow A + B) = \frac{3\beta}{32\pi^2 m_{\sigma_{\tilde{t}}}^2} |R(0)|^2 \frac{1}{1+\delta_{AB}}$$

$$\times \sum_{\lambda_A,\lambda_B} |\mathcal{M}^{\lambda_A,\lambda_B}(\tilde{t}_1 \tilde{t}_1^* \rightarrow AB)|_{v=0}^2 . \tag{5}$$

Here

$$\beta = \left[\left[1 - \frac{m_A^2 + m_B^2}{m_{\sigma_{\tilde{t}}}^2} \right]^2 - \frac{4m_A^2 m_B^2}{m_{\sigma_{\tilde{t}}}^4} \right]^{1/2} \tag{6}$$

is the usual phase space factor and $1/(1+\delta_{AB})$ is a statistics factor. Finally, $R(0)$ is the wave function at the origin. For realistic QCD potentials, the wave function generally has to be computed numerically. Reference [37] provides parametrizations for $R(0)$ as well as the binding energy of the first ten S-wave states of a nonrelativistic (s)quarkonium system, using a potential that describes the known $c\bar{c}$ and $b\bar{b}$ systems well. We will use their parametrizations throughout.

Equation (5) reduces the problem of computing $\sigma_{\tilde{t}_1}$ annihilation decay widths to the calculation of the Feynman amplitude $\mathcal{M}^{\lambda_A \lambda_B}$ for the annihilation of $\tilde{t}_1 + \tilde{t}_1^*$ into $A + B$ with helicities λ_A and λ_B, respectively. Here the initial state is assumed to be a color singlet, and summation over color degrees of freedom of the final state is understood.[4] Since we are only interested in S-wave initial states, we need the Feynman amplitude only in the limit of vanishing relative velocity v of the top squarks; this simplifies the calculation considerably.

We computed the matrix elements for the processes

$$\sigma_{\tilde{t}_1} \rightarrow gg , \tag{7a}$$

$$\sigma_{\tilde{t}_1} \rightarrow W^+ W^- , \tag{7b}$$

$$\sigma_{\tilde{t}_1} \rightarrow ZZ , \tag{7c}$$

$$\sigma_{\tilde{t}_1} \rightarrow Z\gamma , \tag{7d}$$

$$\sigma_{\tilde{t}_1} \rightarrow \gamma\gamma , \tag{7e}$$

$$\sigma_{\tilde{t}_1} \rightarrow hh , \tag{7f}$$

$$\sigma_{\tilde{t}_1} \rightarrow b\bar{b} , \tag{7g}$$

$$\sigma_{\tilde{t}_1} \rightarrow t\bar{t} , \tag{7h}$$

$$\sigma_{\tilde{t}_1} \rightarrow \tilde{Z}_i \tilde{Z}_j, \quad i,j=1,\dots,4 , \tag{7i}$$

where h in Eq. (7f) stands for the light neutral scalar Higgs boson. In general, $\tilde{t}_1 \tilde{t}_1^*$ annihilation can proceed via the four classes (topologies) of Feynman diagrams shown in Fig. 1. The t-channel diagram (a) contributes to all modes of Eq. (7), but with different particles being exchanged: $\tilde{t}_1$ for the gg, $Z\gamma$, and $\gamma\gamma$ final states; $\tilde{t}_1$ and $\tilde{t}_2$ for the ZZ and hh final states; $\tilde{b}_L$ for the $W^+ W^-$ final state; a chargino for the $b\bar{b}$ final state; a neutralino or gluino for the $t\bar{t}$ final state; and a top quark for the $\tilde{Z}_i \tilde{Z}_j$ final state. The u-channel diagram of Fig. 1(b) only contributes if the final state particles do not carry any con-

---

[3]A heavy $\tilde{t}_1$ can also decay into $W + b + \tilde{Z}_1$. We have checked that the corresponding decay width is considerably smaller than the dominant annihilation widths unless the channel (4a) or (4b) is open.

[4]Following Ref. [36], the color wave function of the initial state in Eq. (5) has been normalized such that the color factor is 1 if A and B are singlets under SU(3); this explains the factor of 3 in Eq. (5). See the Appendix for more details.
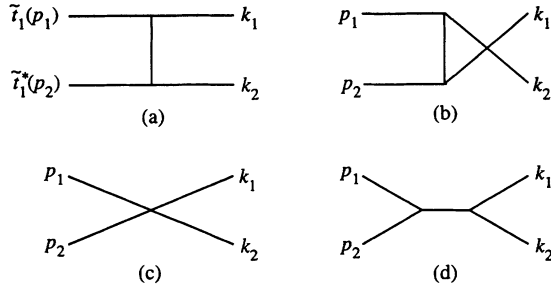
FIG. 1. Four classes of Feynman diagrams that contribute to annihilation decays of top squarkonium into two-body final states.

served charge (reactions 7a,c–f,i); the exchanged particles are then the same as for the t-channel diagram. The four-point diagram of Fig. 1(c) only contributes if the final state particles are bosons (processes 7a–f). Finally, in the limit $v \rightarrow 0$ only the neutral scalar Higgs h, H can be exchanged in the s-channel diagram of Fig. 1(d); this diagram therefore only contributes to reactions (7b,c,f–i). Explicit expressions for the matrix elements for the processes of Eq. (7) are listed in the Appendix.[5]

A first example of $\sigma_{\tilde{t}_1}$ branching ratios is shown[6] in Fig. 2. For clarity, not all final states listed in Eqs. (4) and (7) are represented in this figure. We have fixed $m_t = -\mu = 150$ GeV, $m_{\tilde{t}_L} = m_{\tilde{t}_R} = 200$ GeV, $\tan\beta = 2$, $m_P = 500$ GeV, and $M_2 = 100$ GeV, and have varied A_t between -67 and -312 GeV; since A_t and μ have the same sign, $m_{\sigma_{\tilde{t}}}$ decreases monotonically with increasing $|A_t|$ [see Eq. (3a)].

We see that for this choice of parameters the by far dominant decay mode of $\sigma_{\tilde{t}_1}$ is into two gluons, as long as the single top squark decays (4a) and (4b) are kinematically forbidden. In Fig. 2 the mass of the lighter chargino is around 110 GeV. For $m_{\sigma_{\tilde{t}}} > 2(m_{\tilde{W}_1} + m_b) \simeq 230$ GeV, the decay (4a) (not shown) opens up and quickly dominates over all annihilation decay modes (7). Note, however, that even for $m_{\sigma_{\tilde{t}}} = 400$ GeV the width of the single top squark decay mode (4a) is "only" a few hundred times larger than that for the gg final state; since the partial width for the decay mode (4c) is $\sim 10^{-7}$ smaller than that for (4a), we conclude that this loop decay is entirely negligible as far as $\sigma_{\tilde{t}_1}$ decays are concerned.

---

[5]In principle, the heavy neutral scalar H and pseudoscalar P Higgs bosons can also be produced in top squarkonium decays. For simplicity, we here assume them to be too heavy to contribute, as is the case, e.g., in minimal supergravity models [12]. The corresponding partial widths can be obtained from the hh partial width by replacing some coupling constants.

[6]In this and the following figures, we have set $m_{\sigma_{\tilde{t}}} = 2m_{\tilde{t}_1}$, i.e., have neglected the small reduction of $m_{\sigma_{\tilde{t}}}$ due to the binding energy. This is consistent since the treatment of Refs. [35,36] also neglects the binding energy when computing $\sigma_{\tilde{t}_1}$ decay widths.

Given the large widths for the single top squark decay modes (4a) and (4b), one might worry whether our treatment is adequate for these decays. Inherent to our approach is the assumption that formation and decay of $\sigma_{\tilde{t}_1}$ can be treated separately. This is only true if the $\sigma_{\tilde{t}_1}$ formation time is significantly shorter than its lifetime. A good measure for the (inverse of) the formation time is the binding energy E_{bind} of $\sigma_{\tilde{t}_1}$. For a purely Coulombic potential, the time required to complete one Bohr orbit is proportional to $1/E_{\text{bind}}$, and we expect this relation to survive qualitatively also for the more realistic QCD potential of Ref. [37]. In Fig. 3 we therefore compare the binding energy of the lowest $(1S)$ $\sigma_{\tilde{t}_1}$ state, as parametrized in Ref. [37], with the total $\sigma_{\tilde{t}_1}$ decay width, for two different choices of parameters. In both cases we took $m_t = 150$ GeV, $\tan\beta = 2$, $m_{\tilde{t}_L} = 400$ GeV, $m_{\tilde{t}_R} = 300$ GeV, and $m_P = 500$ GeV; $m_{\sigma_{\tilde{t}}}$ was varied by changing A_t. The solid curve has been obtained with $\mu = -300$ GeV and fixed $M_2 = 100$ GeV. In this case the light chargino is mostly an SU(2) gaugino (W-ino), and the lightest neutralino is mostly a U(1) gaugino (b-ino). Recall that $m_{\tilde{t}_L} > m_{\tilde{t}_R}$ implies that $\tilde{t}_1$ is dominantly an SU(2) singlet $(\cos^2\theta_t < 1/2)$, so that in this scenario the $\tilde{t}_1 \tilde{W}_1 b$ coupling $\propto \cos\theta_t$ is suppressed; $\cos^2\theta_t$ decreases with decreasing $\tilde{t}_L$-$\tilde{t}_R$ mixing and increasing $m_{\tilde{t}_1}$ in this case, which explains the flattening of the solid curve at large $m_{\sigma_{\tilde{t}}}$. We see that in this case the total $\sigma_{\tilde{t}_1}$ decay width is still a factor 3–10 below the binding energy, even well beyond the threshold for decays (4a) and (4b). Our results of Fig. 2, where $\tilde{W}_1$ is also mostly a W-ino, should therefore be at least approximately correct.

In contrast, the dashed curve has been obtained for fixed $\mu = -80$ GeV, while M_2 has been increased along with $m_{\tilde{t}_1}$. The lightest chargino and neutralino states are now both Higgsino-like, and so they couple to $\tilde{t}_L$ and $\tilde{t}_R$ with equal (top Yukawa) strength. The total $\sigma_{\tilde{t}_1}$ decay width therefore increases rapidly with $m_{\sigma_{\tilde{t}}}$; moreover, the opening of the $\tilde{t}_1 \rightarrow t + \tilde{Z}_1$ channel is more pronounced than in the previous case. As a result, $\Gamma(\sigma_{\tilde{t}_1})$ does indeed become comparable to the binding energy in this scenario, which means that our approach will not work for $m_{\sigma_{\tilde{t}}} > 300$ GeV or so. Methods that have recently been developed to describe the $t\bar{t}$ threshold [38] will have to be adopted [39] instead.

Finally, in both cases we observe a very prominent peak at $m_{\sigma_{\tilde{t}}} = 505$ GeV, where the s-channel heavy Higgs boson exchange diagrams become resonant. Since the total decay width of the heavy Higgs boson exceeds the $\sigma_{\tilde{t}_1}$ binding energy, a proper description of this case would have to combine the methods of Ref. [38] with the results of Ref. [40] where the mixing between a nonrelativistic bound state with a (narrow) Higgs resonance is discussed.

The results of Fig. 2 show that the branching ratios for those annihilation decays that might yield a detectable signal for $\sigma_{\tilde{t}_1}$ production at hadron colliders (see Sec. III)
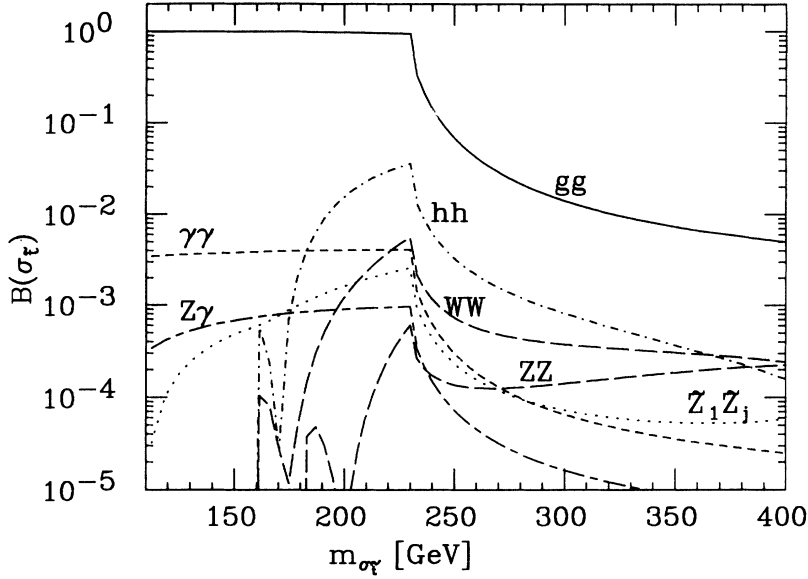
FIG. 2. Branching ratios for annihilation decays of $\sigma_{\tilde{t}_1}$ listed in Eq. (7). The range of $m_{\tilde{t}_1}$ values shown results from varying A_t between -312 and -67 GeV. The values of the other parameters are $m_{\tilde{t}_L} = m_{\tilde{t}_R} = 200$ GeV, $m_t = -\mu = 150$ GeV, $M_2 = 100$ GeV, $m_P = 500$ GeV, and $\tan\beta = 2$. The branching ratios for the $b\bar{b}$ and $t\bar{t}$ final states (not shown) are always below 10^{-3}. The dotted curve only includes $\tilde{Z}_1\tilde{Z}_1$ and $\tilde{Z}_1\tilde{Z}_2$ final states; other neutralino final states are accessible only where $\tilde{t}_1$ has tree-level two-body decays.

become very small if the single top squark decays (4a) and (4b) are allowed; Fig. 3 showed that $\sigma_{\tilde{t}_i}$ may not have time to form at all if there are light Higgsino-like states. In Fig. 4 we have therefore chosen our parameters such that these single top squark decays are kinematically forbidden for $m_{\sigma_{\tilde{t}}} \leq 600$ GeV; this has been obtained by choosing $\mu = -300$ GeV, with the other parameters having the same values as for the dashed curve in Fig. 3. Comparing Fig. 4 with Fig. 2, we note two obvious differences. One is the structure around $m_{\sigma_{\tilde{t}}} = 505$ GeV, which is due to H exchange becoming resonant as already discussed in connection with Fig. 3. Of course, in the immediate vicinity of the resonance our results are not reliable, but the $t\bar{t}$ final state remains dominant in regions of parameter space where $\Gamma(\sigma_{\tilde{t}_1})$ is well below the binding energy.

The other prominent feature of Fig. 4 is the very rapid

increase of the branching ratios for the hh and, to a lesser extent, W^+W^- and ZZ final states. In the case of the hh final state, this can be explained from the observation that in the relevant limit $m_P^2 \gg m_Z^2$ the $h\tilde{t}_1\tilde{t}_1^*$ coupling [41] contains a term $\propto m_t(A_t + \mu\cot\beta)/m_W \propto m_{LR}^2/m_W$, where m_{LR}^2 is again the off-diagonal entry of the top squark mass matrix (1). Moreover, in Fig. 4, $m_{\tilde{t}_L}$ and $m_{\tilde{t}_R}$ are rather large, so that the hh threshold occurs at point where $m_{\tilde{t}_1}^2 \ll m_{\tilde{t}_{L,R}}^2$; Eq. (3a) shows that this also implies $m_{LR}^2 \sim \min(m_{\tilde{t}_L}^2, m_{\tilde{t}_R}^2) \gg m_{\tilde{t}_1}^2$. Close to threshold $\tilde{t}_1$ exchange contribution therefore scales like

$$\mathcal{M}(\tilde{t}_1\tilde{t}_1^* \to hh)\big|_{\tilde{t}_1 \text{ exchange}} \propto \frac{\min(m_{\tilde{t}_L}^4, m_{\tilde{t}_R}^4)}{m_W^2(m_{\tilde{t}_1}^2 - m_h^2/2)},$$

$$m_{\tilde{t}_{L,R}}^2 \gg m_t^2, m_{\tilde{t}_1}^2 \qquad (8)$$
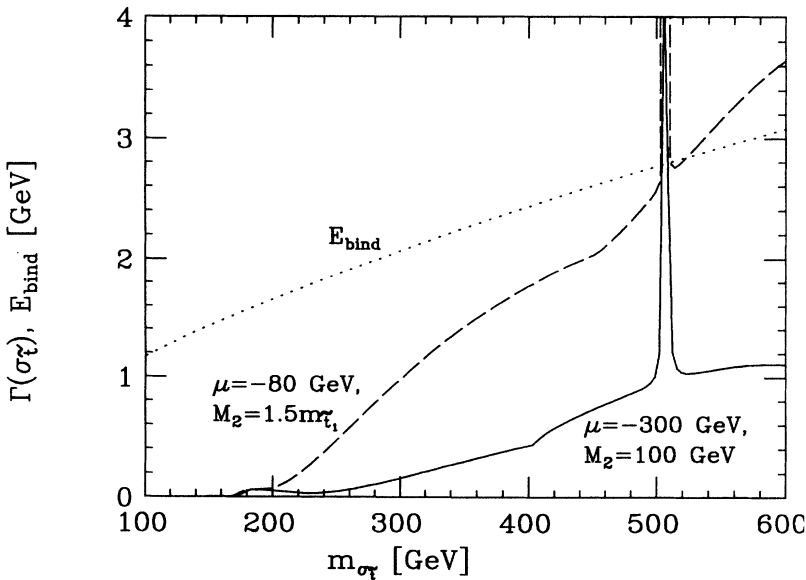
FIG. 3. Binding energy of the lowest top squarkonium state $\sigma_{\tilde{t}_1}$ (dotted curve) is compared with the total $\sigma_{\tilde{t}_1}$ decay width (solid and dashed curves), for two different sets of parameters. We have chosen $m_t = 150$ GeV, $m_P = 500$ GeV, $\tan\beta = 2$, $m_{\tilde{t}_L} = 400$ GeV, and $m_{\tilde{t}_R} = 300$ GeV. The solid and dashed curves correspond to scenarios with a gauginolike and Higgsino-like LSP, respectively.
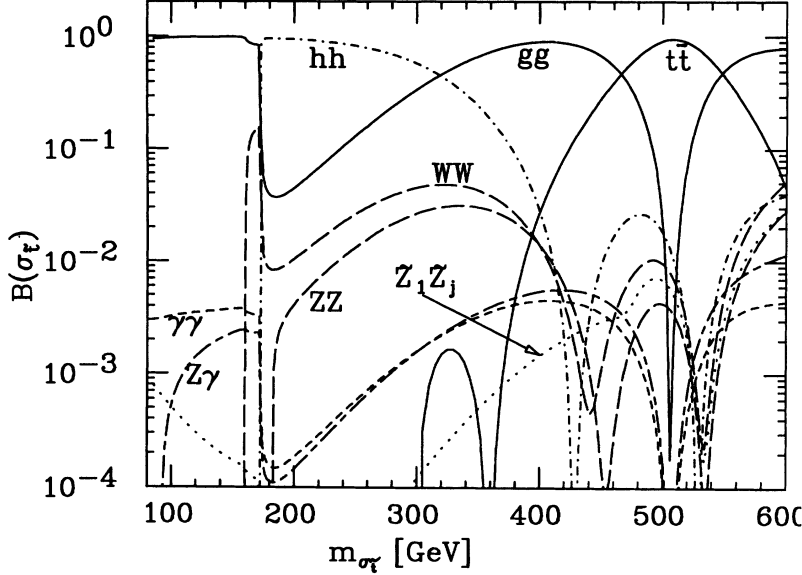
FIG. 4. Branching ratios for annihilation decays of $\sigma_{\tilde{t}_1}$ listed in Eq. (4). The range of $m_{\tilde{t}_1}$ values shown results from varying A_t between 440 and 1080 GeV. We have increased the SU(2) gaugino mass M_2 along with $m_{\tilde{t}_1}$ so that the tree-level single top squark decays of Eq. (3) remain kinematically forbidden $(M_2 = 1.5 m_{\tilde{t}_1})$. The values of the other parameters are $m_t = 150$ GeV, $m_{\tilde{t}_L} = 400$ GeV, $m_{\tilde{t}_R} = -\mu = 300$ GeV, $m_P = 500$ GeV, and $\tan\beta = 2$. The branching ratio for the $b\bar{b}$ mode is again small.

[see Eq. (A9)]; the square of this amplitude clearly decreases very quickly as we move away from the hh threshold ($\propto m_{\tilde{t}_1}^{-4}$). This rapid rise of $\Gamma(\sigma_{\tilde{t}_1} \to hh)$ at the threshold was first observed in[7] Ref. [29].

The behavior of the matrix elements for the W^+W^- and ZZ final states is somewhat more complicated. In the region $m_{\tilde{t}_1}^2 \gg m_W^2$, we can use the equivalence theorem [42] to understand the production of longitudinal gauge bosons, which in this region usually dominates the production of transverse gauge bosons. This theorem states that Feynman amplitudes involving external longitudinal gauge bosons are the same (up to corrections of order $m_W/m_{\tilde{t}_1}$) as those where the gauge bosons are replaced by the corresponding would-be-Goldstone bosons (GB's). These Goldstone modes can also be produced via the Feynman diagrams of Fig. 1. However, it is important to note that the squarks which are exchanged in the t and u channels are *heavy* here. In case of the neutral GB's, only $\tilde{t}_2$ contributes since there are no diagonal couplings between pseudoscalar Higgs boson and top squarks [32]. The corresponding diagrams for charged GB's contain a $\tilde{b}_L$ squark;[8] note that $m_{\tilde{b}_L}$ is linked to $m_{\tilde{t}_L}$ by gauge invariance:

$$m_{\tilde{b}_L}^2 = m_{\tilde{t}_L}^2 - m_W^2 \cos2\beta .\qquad (9)$$

The nonvanishing trilinear scalar couplings of the GB's have similar strength as the $h\tilde{t}_1\tilde{t}_1^*$ coupling; the corresponding t- and u-channel diagrams are therefore at best of order

---

[7]In that paper the $\tilde{t}_2$ exchange contribution to hh production has not been included; this contribution is small where the hh channel is important.

[8]Diagrams with $\tilde{b}_R$ exchange are [32] proportional to m_b^2 and can thus be neglected.

$$\mathcal{M}(\tilde{t}_1\tilde{t}_1^* \to \text{GB's})|_{\tilde{q} \text{ exchange}} \propto \frac{\min(m_{\tilde{t}_L}^4, m_{\tilde{t}_R}^4)}{m_W^2 m_{\tilde{t}_{L,R}}^2} ,$$

$$m_{\tilde{t}_{L,R}}^2 \gg m_t^2, m_{\tilde{t}_1}^2 ,\qquad (10)$$

i.e., are suppressed by a factor of order $(m_{\tilde{t}_1}/m_{\tilde{t}_2})^2$ compared to those for the hh final state. In addition, there are s-channel h exchange contributions

$$\mathcal{M}(\tilde{t}_1\tilde{t}_1^* \to hh, \text{GB's})|_{h \text{ exchange}} \propto \frac{\min(m_{\tilde{t}_L}^2, m_{\tilde{t}_R}^2)}{4m_{\tilde{t}_1}^2 - m_h^2} ,$$

$$m_{\tilde{t}_{L,R}}^2 \gg m_t^2, m_{\tilde{t}_1}^2 .\qquad (11)$$

This contribution exists for both hh and W^+W^- and ZZ final states, but is suppressed by a factor of order $(m_W/m_{\tilde{t}_{L,R}})^2$ compared to the $\tilde{t}_1$ exchange contribution (8) to hh production. Far above the threshold, the width for longitudinal gauge boson production is therefore suppressed by a factor of order $(m_{\tilde{t}_1}/m_{\tilde{t}_2})^4$ compared to the width for the hh final state. Recall that Figs. 2 and 4 have been obtained by varying A_t and hence the $\tilde{t}_1$-$\tilde{t}_2$ mass splitting; the enhancement of the hh mode over the W^+W^- and ZZ modes therefore becomes smaller for large $m_{\sigma_{\tilde{t}}}$.

The equivalence theorem is not applicable close to the W^+W^- and ZZ thresholds. Near the thresholds the t- and u-channel diagrams, which only contribute for longitudinal gauge bosons as shown in Eq. (A3), are suppressed by powers of the phase space factor β of Eq. (6). The four-point and s-channel h exchange diagrams therefore dominate here; the curves of Fig. 2 show that they often interfere destructively. Note that, for $m_{\tilde{t}_1}^2 \ll m_{\tilde{t}_{L,R}}^2$, Eq. (11) also applies approximately for the s-channel contribution to W^+W^- and ZZ production; it

is this term which leads to the rapid increase of the corresponding partial widths near threshold.[9]

Why did Refs. [28] and [30] find so large branching ratios for the W^+W^- final state? The crucial omission is that the relation (9) between $m_{\tilde{b}_L}$ and $m_{\tilde{t}_L}$ has not been taken into account in these papers. We emphasize again that this relation follows directly from SU(2) gauge invariance (and its spontaneous breakdown); it is *independent* of the details of supersymmetry breaking. A violation of Eq. (9) therefore implies explicit (hard) gauge symmetry breaking, which renders the theory nonunitary and/or nonrenormalizable. In addition, $\tilde{t}_L$-$\tilde{t}_R$ mixing has been neglected in these papers. Looking at the exact expression (A3) for $\mathcal{M}(\tilde{t}_1\tilde{t}_1^* \rightarrow W^+W^-)$, it is clear that the cancellation between the t-channel and four-point diagrams, which ensure unitarity in the simple limit $\cos^2\theta_t = 1$, $m_{\tilde{t}_1} = m_{\tilde{t}_L} = m_{\tilde{b}_L}$, can be spoiled if one chooses $m_{\tilde{b}_L}^2 \gg m_{\tilde{t}_1}^2$. However, this implies either $\cos^2\theta_t \rightarrow 0$ (if m_{LR}^2 is kept fixed) or a large s-channel h exchange contribution which again "conspires" to restore unitarity; recall that gauge invariance relates the $h\tilde{t}_1\tilde{t}_1^*$ coupling to the $\tilde{t}_L$-$\tilde{t}_R$ mass splitting and hence to $m_{\tilde{b}_L}$ if $m_{\tilde{t}_L} \simeq m_{\tilde{t}_R}$. In short, the suppression of the partial widths for $\sigma_{\tilde{t}_1} \rightarrow W^+W^-, ZZ$ is a textbook example for the unitarity restoring cancellations that are so characteristic for gauge theories.

Figures 2 and 4 show that the branching ratios for all other modes listed in Eqs. (7) are quite small. The width for the $\gamma\gamma$ final state is simply $8\alpha^2/(9\alpha_s^2)\Gamma(\sigma_{\tilde{t}_1} \rightarrow gg)$, and the partial width for the $Z\gamma$ final state is of similar magnitude or even smaller. (Recall that the $Z\tilde{t}_1\tilde{t}_1^*$ coupling vanishes [15] for $\cos^2\theta_t = \frac{4}{3}\sin^2\theta_W$). For the parameter choices of Figs. 2 and 4, the light neutralinos $\tilde{Z}_{1,2}$ are gauginolike; the partial widths for the $\tilde{Z}_i\tilde{Z}_j$ final states are therefore comparable to those for the $\gamma\gamma$ and $Z\gamma$ final states. Had we chosen the light neutralinos to be Higgsino-like, their partial widths would have been larger by a factor $\propto (m_t/m_W)^4$. For parameter choices leading to mixed-state neutralinos (where both gaugino and Higgsino components are sizable), the s-channel h exchange contribution to $\tilde{Z}_i\tilde{Z}_j$ production can become important, leading to partial widths comparable to those of the W^+W^- and ZZ final states. However, the existence of light Higgsino-like or mixed-state neutralinos in the MSSM also implies a small mass for the light chargino, so that the single top squark decay mode (4a) is allowed, totally swamping all $\sigma_{\tilde{t}_1}$ annihilation decay modes as we have seen above.

Finally, the partial width for the $b\bar{b}$ final state is very small unless $m_{\sigma_{\tilde{t}}} \simeq m_h$ or $\tan\beta \gg 1$. At first glance the gaugino exchange diagram seems to contribute with full SU(2) gauge strength. However, chirality implies that $\Gamma(\sigma_{\tilde{t}_1} \rightarrow f\bar{f}) \propto m_f^2$ for any SM fermion f. As a result, the

$b\bar{b}$ final state can be important only if the b-quark Yukawa coupling is enhanced ($\tan\beta \gg 1$) or in the immediate vicinity of the h resonance. Figure 4 shows that even the partial width for the $t\bar{t}$ final state is quite small away from the H pole. This is partly due to destructive interference between s- and t-channel diagrams for $m_{\sigma_{\tilde{t}}} < m_H$ and partly because color factors suppress all t-channel contributions [see Eq. (A14)].

We thus conclude that, if the tree-level single top squark decays (4a) and (4b) are kinematically forbidden and $m_{\sigma_{\tilde{t}}}$ is not close to either m_h or m_H, the total $\sigma_{\tilde{t}_1}$ decay width is dominated either by the gg or hh partial width, with the W^+W^- and ZZ partial widths playing a secondary role. Our discussion of Fig. 4 already showed that the ratio of the gg to hh partial widths crucially depends on the size of the LR element of the top squark mass matrix (1). This is further illustrated in Fig. 5, where we show the gg, hh, and W^+W^- partial widths as a function of $m_{\sigma_{\tilde{t}}}$ for three different choices of parameters. We have fixed $\mu = 500$ GeV, $m_P = 1$ TeV, and $m_t = 150$ GeV; instead of varying A_t, we have fixed the dimensionless quantity $A \equiv 2A_t/(m_{\tilde{t}_L} + m_{\tilde{t}_R})$, as well as the ratio $m_{\tilde{t}_R}/m_{\tilde{t}_L}$, and varied $m_{\tilde{t}_L}$. The dependence of the hh and W^+W^- partial widths on $m_{\sigma_{\tilde{t}}}$ is therefore quite different than[10] in Figs. 2 and 4. In particular, Eq. (3a) implies that now m_{LR}^2, and hence the strength of the $h\tilde{t}_1\tilde{t}_1^*$ coupling, increases with increasing $m_{\sigma_{\tilde{t}}}$ even if $m_{\tilde{t}_1}^2 \ll m_{\tilde{t}_{L,R}}^2$. For large A the hh partial width still decreases with increasing $m_{\sigma_{\tilde{t}}}$, due the $\tilde{t}_1$ propagator suppression, but the decline is much less rapid than in Fig. 4. Note that we have chosen $\mu > 0$ here, so that m_{LR}^2 increases monotonically with increasing A. However, because of destructive interference between different diagrams, both the hh and the W^+W^- partial width initially decrease with increasing m_{LR}^2, shooting up quickly once $A > 1$. We have already seen above that the partial width for the W^+W^- final state always stays well below those for the hh and gg final states. Here we see that the off-diagonal entries of the top squark mass matrix (1) need not be all that large for the hh mode to dominate $\sigma_{\tilde{t}_1}$ decays. Finally, the short-dashed curve has been obtained with $m_{\tilde{t}_L} = m_{\tilde{t}_R}$, as compared to $m_{\tilde{t}_R} = 0.7m_{\tilde{t}_L}$ for the other curves; we see that this has only little effect on $\Gamma(\sigma_{\tilde{t}_1} \rightarrow hh)$. Since we kept A fixed, the size of m_{LR}^2 for given $m_{\tilde{t}_1}$ is about the same for the two choices of $m_{\tilde{t}_R}/m_{\tilde{t}_L}$; this again indicates that the size of m_{LR}^2 is indeed the quantity that decides whether or not the hh partial width is sizable. We will come back to this point later.

---

[9]The coupling of the heavy scalar Higgs boson H to W and Z bosons is suppressed [32] for $m_P^2 \gg m_W^2$.

[10]Of course, the gg partial width is fixed uniquely by m_{σ_i} and the strength of the QCD coupling constant and is hence the same for all three cases.
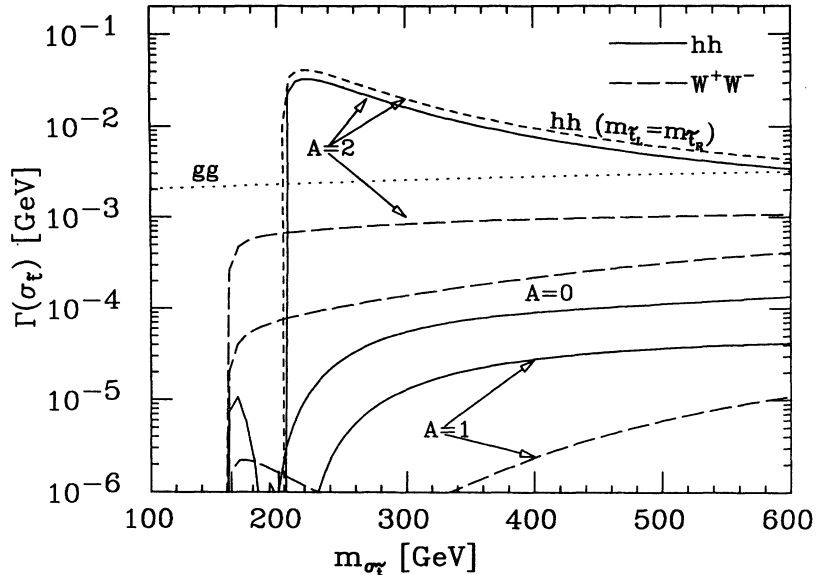
FIG. 5. Dominant partial widths for $\sigma_{\tilde{t}_1}$ annihilation decays. The gg partial width (dotted curve) depends only on $m_{\tilde{t}_1}$ and the QCD scale parameter Λ, while the hh (solid and short-dashed curves) and W^+W^- (long-dashed curves) partial widths in general depend on all parameters entering the top squark mass matrix of Eq. (1). We have kept $A \equiv 2A_t/(m_{\tilde{t}_L} + m_{\tilde{t}_R})$ as well as the ratio $m_{\tilde{t}_L}/m_{\tilde{t}_R}$ fixed and varied $m_{\tilde{t}_L}$. Most curves are for $m_{\tilde{t}_R} = 0.7 m_{\tilde{t}_L}$, but the short-dashed curve has been obtained with $m_{\tilde{t}_R} = m_{\tilde{t}_L}$. The values of the other parameters are $m_t = 150$ GeV, $\tan\beta = 3$, $\mu = 500$ GeV, and $m_P = 1$ TeV.

Having completed our discussion of $\sigma_{\tilde{t}_1}$ decays, we are now ready to study possible signals for its production at hadron colliders.

III. SIGNALS FOR TOP SQUARKONIUM PRODUCTION

In this section we discuss how one might search for $\sigma_{\tilde{t}_1}$ states. We focus on hadron (super)colliders, since they offer the largest cross sections; furthermore, the machines we discuss either already exist (Tevatron) or are in a relatively advanced stage of planning [CERN Large Hadron Collier (LHC)], while plans for future linear e^+e^- or $\gamma\gamma$ colliders are still at a very preliminary stage. The production of $\sigma_{\tilde{t}_1}$ at hadron colliders proceeds via gluon fusion. This process is related by crossing to the $\sigma_{\tilde{t}_1} \to gg$ decay, whose partial width we computed in the previous section. The total cross section for $\sigma_{\tilde{t}_1}$ production is then (to leading order in the QCD coupling constant) simply given by

$$\sigma(pp \to \sigma_{\tilde{t}_1} + X)$$

$$= \int_\tau^1 \frac{dx}{x} \tau G(x, Q^2) G\left(\frac{\tau}{x}, Q^2\right) \frac{\pi^2}{8m_{\sigma_{\tilde{t}}}^3} \Gamma(\sigma_{\tilde{t}_1} \to gg) ,$$

(12)

where $\tau \equiv m_{\sigma_{\tilde{t}}}^2/s$ with s being the squared pp invariant energy; since in leading order only gluon fusion contributes, the cross section is the same for pp and $p\bar{p}$ colliders. Unless stated otherwise we have used the parametrization of Ref. [43] for the gluon distribution functions G and have chosen the scale $Q = m_{\tilde{t}_1}$. In order to set the stage for the subsequent discussion, we remark here that Eq. (12) predicts a total $\sigma_{\tilde{t}_1}$ production cross section at the LHC ($\sqrt{s} = 14$ TeV) of 80 (22,8.5) pb for $m_{\sigma_{\tilde{t}}} = 150$ (200,250) GeV.

Unfortunately, most $\sigma_{\tilde{t}_1}$ decays will not lead to a signal that is detectable at hadron colliders. To begin with, the QCD dijet cross section integrated over any reasonable invariant-mass window will be many orders of magnitude larger than the total $\sigma_{\tilde{t}_1}$ production cross section, making it impossible to detect $\sigma_{\tilde{t}_1} \to gg$ decays. QCD backgrounds also swamp $\sigma_{\tilde{t}_1} \to b\bar{b}, t\bar{t}$ decays. Single top squark $\tilde{t}_1 \to b + \tilde{W}_1$ decays can give hard, isolated leptons in the final state if $\tilde{W}_1$ decays leptonically. However, the open $\tilde{t}_1 \tilde{t}_1^*$ pair production cross section [14] is some four orders of magnitude larger than the $\sigma_{\tilde{t}_1}$ cross section. The presence of two invisible LSP's and at least one neutrino in the $\sigma_{\tilde{t}_1} \to \tilde{W}_1 + \tilde{W}_1^- b\bar{b} \to l^\pm X$ signal makes it impossible to reconstruct $m_{\sigma_{\tilde{t}}}$ even in principle. We conclude that single top squark decays will never give a signal for $\sigma_{\tilde{t}_1}$ production at hadron colliders even if conditions are favorable for the detection of open top squark production [14].

In Ref. [30] the use of the W^+W^- decay mode (for rather heavy $\sigma_{\tilde{t}_1}$, to be produced at future supercolliders) was advocated. However, we have seen in the previous section that in this paper the $B(\sigma_{\tilde{t}_1} \to W^+W^-)$ was overestimated by a large factor. Moreover, this final state can only compete with QCD backgrounds if both W bosons decay leptonically. The event will then contain two neutrinos, which make it impossible to reconstruct the invariant mass of the W^+W^- system. Even if it were possible to somehow discriminate against the enormous $t\bar{t}$ background at hadron supercolliders, the continuum cross section for W^+W^- production is still at least an order of magnitude larger [44] than the $\sigma_{\tilde{t}_1} \to W^+W^-$ signal.

The authors of Ref. [29] proposed to use the $\sigma_{\tilde{t}_1} \to hh \to \tau^+\tau^+\tau^-\tau^-$ decay as a signal. This might have been feasible for light $\sigma_{\tilde{t}_1}$ and light h at the Tevatron collider. Unfortunately, the lower bound on m_h from

Higgs searches at the CERN e^+e^- collider LEP [45] excludes this possibility for $\sigma_{\tilde{\tau}_1}$ light enough to be produced at the Tevatron. The $\tau^+\tau^+\tau^-\tau^-$ SM background is much larger at supercollider energies, making it considerably more difficult to observe a $\sigma_{\tilde{\tau}_1}$ signal in this channel. For example, at the LHC ($\sqrt{s}=14$ TeV) the $ZZ \rightarrow 4\tau$ background amounts [44] to approximately 10 fb. Using [46] $B(h \rightarrow \tau^+\tau^-) = 10\%$, we find that the $\sigma_{\tilde{\tau}_1} \rightarrow 4\tau$ signal could be as large as 1 pb if $m_{\sigma_{\tilde{\tau}}} \leq 150$ GeV and $B(\sigma_{\tilde{\tau}_1} \rightarrow hh) \simeq 1$. While this is considerably larger than the most narrowly defined physics background, it is smaller than the cross section for $pp \rightarrow b\bar{b}b\bar{b} \rightarrow 4\tau$ production.[11] One might be able to reduce this particular background, e.g., by requiring the four τ leptons not to occur as two back-to-back pairs. The real question, however, is how reliable a τ lepton can be identified at the LHC. In particular, it is at present not clear how often events containing jets with low charged particle multiplicity might fake τ signals. Note that the presence of (at least four) neutrinos in the final state makes it once again impossible to reconstruct either m_h or $m_{\sigma_{\tilde{\tau}}}$. While the rate can be tantalizingly large, isolation of the $\tau^+\tau^+\tau^-\tau^-$ signal at a hadron supercollider could therefore be quite difficult; certainly, detailed Monte Carlo simulations would have to be performed before a good case for this signal can be made.

This leaves us with $\sigma_{\tilde{\tau}_1}$ decay modes with rather small branching ratios. The $\tilde{Z}_i \tilde{Z}_j$ mode again suffers from the problem that $m_{\sigma_{\tilde{\tau}}}$ cannot be reconstructed since the final state contains two LSP's. The ZZ mode offers a clean signal if both Z bosons decay leptonically. Unfortunately, the branching ratio for the ZZ final state is often quite small, as shown in Figs. 2 and 4. The conditions for this signal are most favorable for large LR element of the top squark matrix (1) and in the mass range $m_h \geq m_{\tilde{\tau}_1} > m_Z$. In this case, $B(\sigma_{\tilde{\tau}_1} \rightarrow ZZ)$ can be as large as 10%, giving a maximal $\sigma(pp \rightarrow \sigma_{\tilde{\tau}_1} \rightarrow l^+l^+l^-l^-X) \simeq 8$ fb for $m_{\sigma_{\tilde{\tau}}} = 200$ GeV at $\sqrt{s} = 14$ TeV, corresponding to 800 events in a full LHC year ($\int \mathcal{L} \, dt = 100$ fb^{-1}); this should be readily detectable. However, since in the MSSM m_h cannot be larger than 140 GeV or so even after the inclusion of radiative corrections [33,34], this window of opportunity is rather narrow. Figures 2 and 4 show that more generically the ZZ branching ratio lies between 0.1% and 1%, making this signal rather marginal; recall that, in the SM, $\sigma(pp \rightarrow ZZ \rightarrow l^+l^+l^-l^-X) \simeq 40$ fb [44] at the LHC. We should mention here that observability of the $\sigma_{\tilde{\tau}_1} \rightarrow ZZ \rightarrow 4l$ signal largely depends on the energy resolution of the detector, since the natural width of $\sigma_{\tilde{\tau}_1}$

---

[11]This is true for the high luminosity option of the LHC, where most $4b$ events originate from independent pp collisions. The $4b \rightarrow 4\tau$ background for low luminosities is [47] around 0.2 pb.

is very small, as we saw above. If the resolution is very good, the signal would be essentially rate limited. For poorer resolution it might be worthwhile to also consider the case where only one of the two Z bosons decays leptonically while the other decays into neutrinos. The signal would then be the Jacobian peak in the transverse momentum distribution of the visible Z boson. Even here the rate will be quite small once $m_{\tilde{\tau}_1} > m_h$; in the accessible region, the transverse momentum of the Z bosons will therefore not be large. One will then have to worry about single Z backgrounds with some amount of "fake" missing transverse momentum.

The $Z\gamma$ final state could also give a clean signal if $Z \rightarrow l^+l^-$. Unfortunately, the combined branching ratio for $\sigma_{\tilde{\tau}_1} \rightarrow Z\gamma \rightarrow l^+l^-\gamma$ is always below 0.01%. Note that photons have to be quite energetic to yield a potential signal at the LHC; this final state can therefore only be used for $m_{\sigma_{\tilde{\tau}}} > 150$ GeV or so. The total $pp \rightarrow \sigma_{\tilde{\tau}_1} \rightarrow Z\gamma \rightarrow l^+l^-\gamma$ signal than amounts to at most 10 fb at $\sqrt{s} = 14$ TeV; in comparison, the SM physics background [48] is about 600 fb even if one requires the transverse momentum of the photon to exceed 50 GeV. It seems therefore very unlikely to us that this signal will be detectable.

Such considerations led us to propose [31] the $\gamma\gamma$ final state as the most promising signal for $\sigma_{\tilde{\tau}_1}$ production at hadron colliders. Figures 2 and 4 show that the corresponding branching ratio is typically a few times 10^{-3}, although it can be substantially smaller near an s-channel pole or for large m_{LR}^2; this is considerably larger than typical branching ratios into leptonically decaying Z bosons. Since the $\sigma_{\tilde{\tau}_1} \rightarrow \gamma\gamma$ partial width is determined uniquely by $m_{\tilde{\tau}_1}$ (for a given QCD potential), the $\gamma\gamma$ signal rate depends on model parameters only via the total $\sigma_{\tilde{\tau}_1}$ decay width. The signal is very simple, consisting of two hard photons with invariant mass $M_{\gamma\gamma} = m_{\sigma_{\tilde{\tau}}}$ in a hadronically quiet event. Of course, there is also a sizable SM background from $q\bar{q}$ annihilation and gg fusion. It has been studied in some detail in the literature [49,50] as a background to a possible signal for intermediate mass Higgs boson production. Recall that the natural width of the signal peak in our case is just a few MeV (see Fig. 5); in contrast, the background gives a smooth distribution in $M_{\gamma\gamma}$. The question is then if, or under what circumstances, the signal peak is observable on top of the background.

In most SM $\gamma\gamma$ events, the photons will emerge at small angles, due to t- and u-channel quark propagator effects; in contrast, the signal is isotropic in $\cos\theta^*$, where θ^* is the scattering angle in the $\gamma\gamma$ center-of-mass system. We therefore impose the cut

$$|\cos\theta^*| \leq 0.5 \, . \tag{13}$$

The $\gamma\gamma$ background has been computed to next-to-leading order (NLO) in QCD [50]. However, if one vetoes against the presence of hard, central jets in the event and requires the photons to be isolated, the NLO prediction for the background rate is actually very simi-

lar to the leading order estimate. Moreover, no NLO calculation for the signal cross section exists as yet. We therefore also treat the background in leading order, but we include the $gg \rightarrow \gamma\gamma$ contribution which has been found to be very important [49] especially for low $M_{\gamma\gamma}$.

As noted above, the natural width of the signal peak is extremely small; however, because of the detector resolution effects, its actual (measured) width will be much larger. Clearly, the background should be integrated over this large range of $M_{\gamma\gamma}$. On the other hand, the signal within a given bin need not be larger than the background in order to be detectable, since the expected background level can be determined experimentally by fitting a smooth function to the sidebins. The question is then whether the excess in the signal bin is statistically significant or not. Following Ref. [51], where the search for SUSY Higgs bosons was discussed, we define the signal to be significant if the 99% C.L. upper limit on the background rate is smaller than the 99% C.L. lower limit on signal plus background combined. In the limit of large event numbers, where Gaussian statistics can be used, this means

$$N_b + N_s - 2.32\sqrt{N_b + N_s} \geq N_b + 2.32\sqrt{N_b} \ , \qquad (14)$$

which implies

$$N_s \geq 2.32(2\sqrt{N_b} + 2.32) \ . \qquad (15)$$

Here N_b and N_s are the expected number of signal and background events after cuts. As noted earlier, the background has to be integrated over a detector-dependent bin width $\Delta M_{\gamma\gamma}$:

$$N_b = \left[\int \mathcal{L} \, dt \right] \frac{d\sigma_b}{dM_{\gamma\gamma}} \bigg|_{M_{\gamma\gamma} = m_{\sigma_{\tilde{t}}}} \Delta M_{\gamma\gamma} \ . \qquad (16)$$

In the limit $\sqrt{N_b} \gg 1$, the minimal detectable signal cross section $\sigma_{\gamma\gamma}^{\min} = N_s / (\int \mathcal{L} \, dt)$ therefore scales like the inverse square root of the integrated luminosity and also

like the inverse square root of the energy resolution of the electromagnetic calorimeter, which determines the size of $\Delta M_{\gamma\gamma}$. In our background estimates, we simply took $\Delta M_{\gamma\gamma}$ to be twice the assumed invariant mass resolution.

In Fig. 6 we show the expected signal at the Tevatron ($\sqrt{s} = 1.8$ TeV). In addition to the cut (13), we have required that both photons have rapidity $|y_\gamma| \leq 1.1$, so that $|\cos\theta_\gamma| \leq 0.8$ in the laboratory frame; the same cut has been applied by the Collider Detector at Fermilab (CDF) Collaboration in their preliminary analysis [52] of events with two hard photons. The dashed curve has been obtained under the assumption that the total width of $\sigma_{\tilde{t}_1}$ is determined by the gg and $\gamma\gamma$ partial widths alone, while for the solid curve all $\sigma_{\tilde{t}_1}$ decay modes of Eq. (7) have been included. The two results are indistinguishable except for $m_{\sigma_{\tilde{t}}} \simeq m_h = 87$ GeV for the given choice of parameters. The signal for such light $\sigma_{\tilde{t}_1}$ does therefore not depend on the details on the (s)particle spectrum (aside from $m_{\tilde{t}_1}$) as long as $\tilde{t}_1$ has no tree-level two-body decays and s-channel h exchange contributions to $\sigma_{\tilde{t}_1}$ decays are not "accidentally" enhanced.

In Fig. 6 we also show our estimates for the minimal detectable signal cross section (dotted lines) for three different values of the integrated luminosity representing the present status (18 pb^{-1}), the hoped-for luminosity after run Ib (100 pb^{-1}), and an estimate of what might be achievable after the new Main Injector has been completed (1 fb^{-1}). Here we have assumed an invariant-mass resolution of 2%, i.e., $\Delta M_{\gamma\gamma} = 0.04 M_{\gamma\gamma}$; this is the constant term in the energy resolution of the electromagnetic calorimeter of the CDF detector [52]. Since the expected number of background events per bin is not always large, we have used Poissonian statistics to derive these curves; however, Eq. (15) gives quite similar results in the mass range where detection of $\sigma_{\tilde{t}_1}$ might be possible.

We conclude from Fig. 6 that the mass reach of the
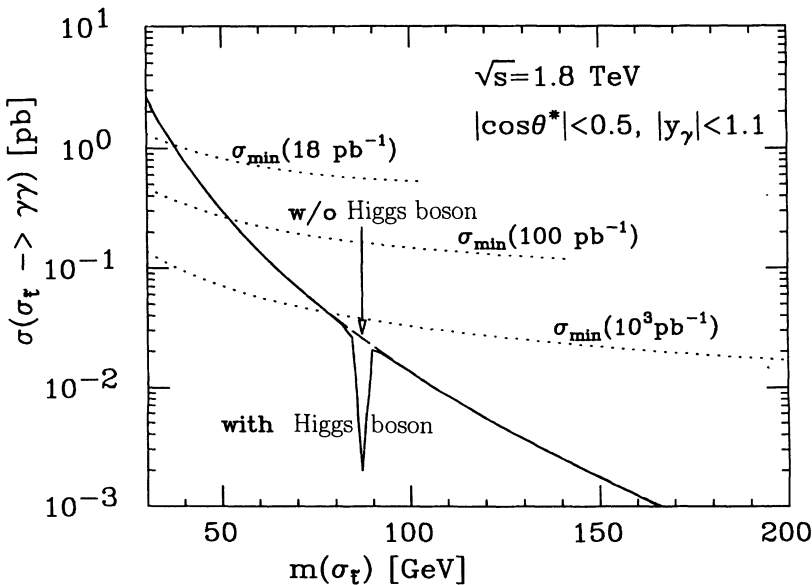
FIG. 6. Cross section for $p\bar{p} \rightarrow \sigma_{\tilde{t}_1} \rightarrow \gamma\gamma$ after cuts at the Tevatron. The dashed curve assumes $\Gamma_{\text{tot}}(\sigma_{\tilde{t}_1}) = \Gamma(\sigma_{\tilde{t}_1} \rightarrow gg)$, while the solid line includes all channels listed in Eqs. (7); the difference is noticeable only for $m_{\sigma_{\tilde{t}}} \simeq m_h$. The dotted curves show our estimates of the minimal signal that is visible on top of the smooth $\gamma\gamma$ background for three different values of the integrated luminosity. The signal has been computed for $m_t = 150$ GeV, $\tan\beta = 2$, $M_2 = 1.5 m_{\tilde{t}_1}$, $m_{\tilde{t}_L} = 1.5 m_{\tilde{t}_R} = 300$ GeV, $m_P = 500$ GeV, and $\mu = -133$ GeV.

Tevatron for $\sigma_{\tilde{t}_1}$ searches is quite modest. It is therefore exceedingly unlikely that one of the two CDF events [52] with very large $M_{\gamma\gamma}$ (350 and 430 GeV, respectively) is due to $\sigma_{\tilde{t}_1}$ production. Indeed, most of the region that one might be able to probe even with an integrated luminosity of 1 fb^{-1} is already excluded by LEP measurements of the total Z decay width and/or squark searches at LEP, *unless* the $Z\tilde{t}_1\tilde{t}_1^*$ coupling happens to be suppressed by $\tilde{t}_L$-$\tilde{t}_R$ mixing. On the other hand, Fig. 6 also reveals that *existing* Tevatron data might already help to probe this light top squark window; in particular, they might confirm or rule out the recently proposed explanation [17] of the (small) excess of events containing low-p_T D^* mesons observed [16] by the TOPAZ Collaboration in terms of $\tilde{t}_1\tilde{t}_1^*$ production and subsequent $\tilde{t}_1 \rightarrow c + \tilde{Z}_1$ decay with $m_{\tilde{t}_1} \simeq 15$ GeV and $m_{\tilde{Z}_1} \simeq 12.5$ GeV.

In Fig. 7 we show results for LHC energy ($\sqrt{s} = 14$ TeV). We have again applied the cut (13) on $\cos\theta^*$, but have relaxed the requirement for y_γ slightly compared to Fig. 6; our cut $|y_\gamma| \leq 1.74$ still ensures that the photons are at least 20° away from the beam pipes, i.e., are well isolated from the beam remnant jets. We have also rather optimistically assumed a 1% resolution for the measurement of $M_{\gamma\gamma}$, i.e., used Eq. (16) with $\Delta M_{\gamma\gamma} = 0.02 M_{\gamma\gamma}$. Since now the expected number of background events per bin is quite large, we have used Gaussian statistics to estimate the minimal detectable signal $\sigma_{\gamma\gamma}^{min}$; the dotted curve shown in Fig. 7 assumes one nominal LHC year of operations, i.e., $\int \mathcal{L}\, dt = 100$ fb^{-1}.

The solid line in Fig. 7 shows the total $\sigma_{\tilde{t}_1}$ production cross section (divided by 100), without any cuts. The dashed curves show the $\gamma\gamma$ signal cross sections after cuts for the two sets of parameters chosen in Figs. 2 and 4. We saw in Sec. II that the branching ratio for the $\gamma\gamma$ mode is about 3×10^{-3} at small $m_{\sigma_{\tilde{t}}}$, where the gg mode dominates. Comparing the solid and dashed lines in Fig.

7, we see that our cuts reduce the signal by approximately a factor of 3.5 at low $m_{\sigma_{\tilde{t}}}$; at high $m_{\sigma_{\tilde{t}}}$, almost half of all $\sigma_{\tilde{t}_1} \rightarrow \gamma\gamma$ events pass. Of course, the cut (13) alone excludes 50% of all signal events; for large $m_{\sigma_{\tilde{t}}}$, the events are automatically central so that the cut on the rapidity does not reduce the event number further. The reduction of the $q\bar{q}, gg \rightarrow \gamma\gamma$ backgrounds by our cuts is much larger; in addition, we have to require the photons to be well isolated from all jet activity, including the beam remnant jets, in order to suppress the bremsstrahlung background, which otherwise dominates [49].

The short-dashed curve shows that, as anticipated, the $\gamma\gamma$ signal quickly becomes unobservable once $\tilde{t}_1$ has tree-level two-body decays ($m_{\sigma_{\tilde{t}}} > 230$ GeV; see Fig. 2). Here the situation is quite analogous to the case of $t\bar{t}$ bound state production where the $\gamma\gamma$ signal also becomes inaccessible [53] once $m_t > 120$ GeV or so. The rapid decline of the long-dashed curve in Fig. 7 at $m_{\sigma_{\tilde{t}}} = 180$ GeV is due to the opening of the hh mode (see Fig. 4). In this case the $\gamma\gamma$ signal becomes marginal just beyond the hh threshold, but should still be observable after several years of LHC operations if our assumptions about the detector resolution can be realized. Note that the signal actually increases with increasing $m_{\sigma_{\tilde{t}}}$ as we leave the hh threshold region, in spite of the rapid decrease of the total cross section for $\sigma_{\tilde{t}_1}$ production; this once again illustrates the steep decline of the hh partial width with decreasing m_{LR}^2, which corresponds to increasing $m_{\tilde{t}_1}$ in this case as discussed in Sec. II. Finally, for $m_{\sigma_{\tilde{t}}} \simeq m_H$ the $\gamma\gamma$ signal again becomes unobservable, due to the large s-channel enhancement of the $t\bar{t}$ partial width.

Before we try to further evaluate the top squarkonium discovery potential of the LHC, it might be worthwhile to discuss some of the uncertainties inherent to our calculation of signal rates. As stated earlier, the cross sections shown in Figs. 6 and 7 have been computed using the pa-
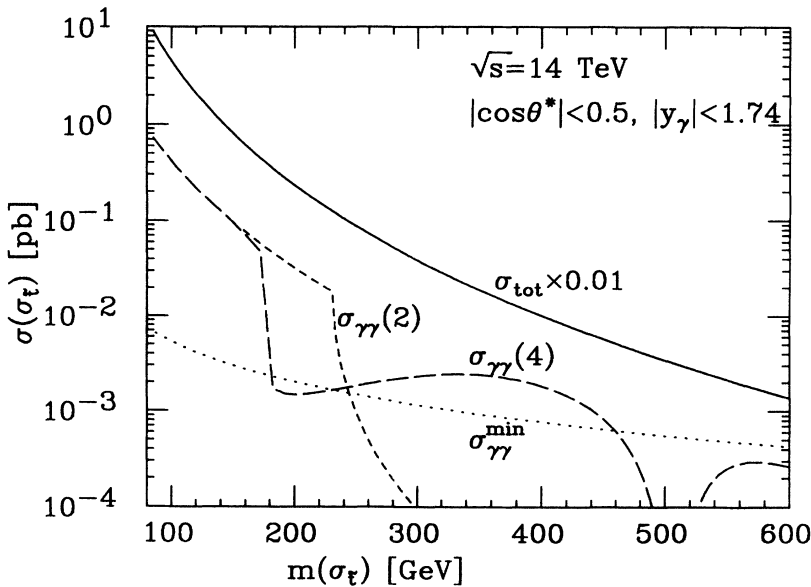
FIG. 7. Cross section for $\sigma_{\tilde{t}_1}$ production at the LHC. The solid line shows the total cross section multiplied by 0.01 and the dashed curves the $\gamma\gamma$ signal cross section after cuts for the two scenarios of Figs. 2 and 4. The dotted curve shows the minimal cross section giving a significant signal after 1 year of nominal LHC operations, as defined in the text.

rametrization of the parton distribution functions in the proton given by Owens [43]; we found that other parametrizations [54] give very similar results. Our cut on the rapidity of the photon ensures that we probe the gluon density G at comparatively large values of x where differences between existing parametrizations are not so large. In our previous figures, we have taken $Q = m_{\tilde{t}_1}$ for the momentum scale in the gluon distribution function; the same choice has been used for the solid and dashed curves in Fig. 8. In contrast, the dotted curve has been obtained with $Q = m_{\sigma_{\tilde{t}}}$. Clearly, this change of Q by a factor of 2 has little effect on the predicted signal rate. For small (large) values of x, the gluon density increases (decreases) as Q is increased; most of our signal comes from the crossover region in between, where G depends very weakly on Q. We note here that we have not changed the scale in α_s in Fig. 8, which determines $\Gamma(\sigma_{\tilde{t}_1} \to gg)$ and hence the total $\sigma_{\tilde{t}_1}$ production cross section [see Eq. (12)]. However, for the given choice of parameters the total $\sigma_{\tilde{t}_1}$ decay width is always dominated by the gg partial width, so that the branching ratio for the $\gamma\gamma$ final state is inversely proportional to $\Gamma(\sigma_{\tilde{t}_1} \to gg)$; the signal is therefore almost independent of the choice of the momentum scale to be used in α_s in the given case.

Nevertheless, our results do depend on the choice of the QCD scale Λ, as also shown in Fig. 8. The reason is that larger values of Λ imply a bigger QCD coupling constant α_s and hence a more tightly bound top squarkonium system, i.e., larger $|R(0)|^2$; note that the signal is $\propto |R(0)|^2$ if the total $\sigma_{\tilde{t}_1}$ decay width is dominated by annihilation decays. Reference [37] provides parametrizations of this quantity for four different values of Λ; our previous results have been obtained with $\Lambda = 0.2$ GeV, which is in between the extreme choices of 0.1 and 0.4 GeV. We see that even for $\Gamma_{\text{tot}}(\sigma_{\tilde{t}_1}) \simeq \Gamma(\sigma_{\tilde{t}_1} \to gg)$ the variation of Λ corresponds to a 30% uncertainty of our

signal. This uncertainty is even larger if $\Gamma_{\text{tot}}(\sigma_{\tilde{t}_1}) \gg \Gamma(\sigma_{\tilde{t}_1} \to gg)$. If the total width is dominated by annihilation decays into hh or $t\bar{t}$ final states, the uncertainty in Λ leads to an approximately 50% uncertainty of the signal, since now the increase of the gg partial width, i.e., of the total cross section for $\sigma_{\tilde{t}_1}$ production, is no longer canceled by a corresponding decrease of the branching ratio for the $\gamma\gamma$ final state when Λ is increased. The Λ dependence becomes stronger yet if tree-level two-body decays of $\tilde{t}_1$ are possible, since in this case the signal is

$$ \propto \Gamma(\sigma_{\tilde{t}_1} \to gg)\Gamma(\sigma_{\tilde{t}_1} \to \gamma\gamma)/\Gamma_{\text{tot}}(\sigma_{\tilde{t}_1}) \propto \alpha_s^2 |R(0)|^4 \; ; $$

the signal now increases by more than a factor of 4 when Λ is increased from 0.1 to 0.4 GeV. A similarly strong dependence on Λ was observed in Ref. [53] for the analogous case of the $\gamma\gamma$ signal for top quarkonium production. However, Fig. 7 shows that detection of $\sigma_{\tilde{t}}$ at the LHC becomes much more difficult if $\Gamma_{\text{tot}}(\sigma_{\tilde{t}_1}) \gg \Gamma(\sigma_{\tilde{t}_1} \to gg)$ and all but impossible if $\tilde{t}_1$ has unsuppressed tree-level two-body decays. The situation depicted in Fig. 8 is therefore more characteristic for situations where the discovery of $\sigma_{\tilde{t}_1}$ seems feasible at the LHC.

Yet another uncertainty comes from the existence of higher (excited) top squarkonium states. So far, we have only considered the direct production of the lowest-lying $(n = 1)$ state. However, already for the $c\bar{c}$ system two $(J = 1)$ S-wave bound states are known to exist; there are three $J = 1$ s-wave $b\bar{b}$ bound states. For a Coulomb potential, the number of bound states increases proportional to the square root of the mass of the heavy (s)quark. As mentioned earlier, in Ref. [37] the mass (binding energy) and wave function at the origin of the first ten heavy (s)quarkonium states are given (the ground state and nine excited states). Not all of these states will be true bound states; some may be resonances that decay rapidly into a pair of top-squark-flavored (spin-$\frac{1}{2}$) "mesons." We as-
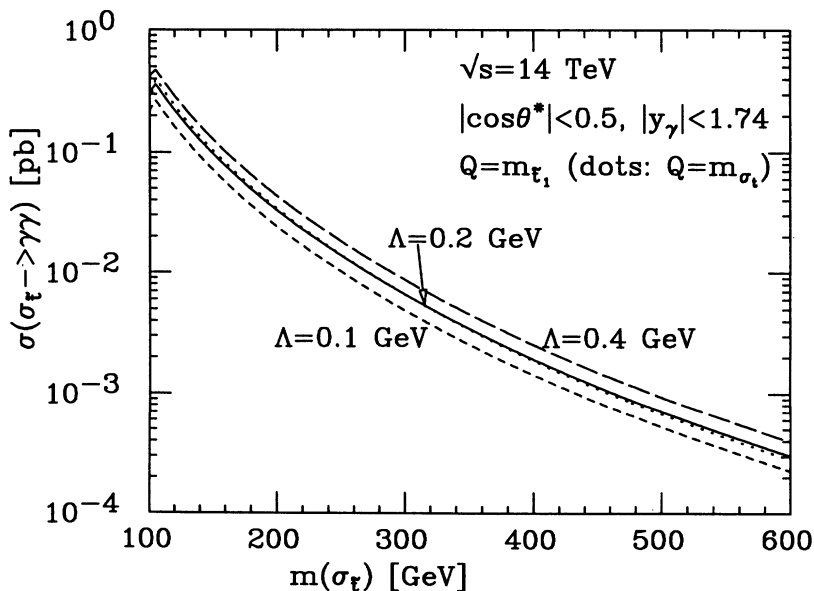
FIG. 8. Dependence of the $\gamma\gamma$ signal cross section after cuts on the choice of the scale Q in the gluon distribution functions and on the QCD parameter Λ. The parameters are as in Fig. 5, with $A = 1$.
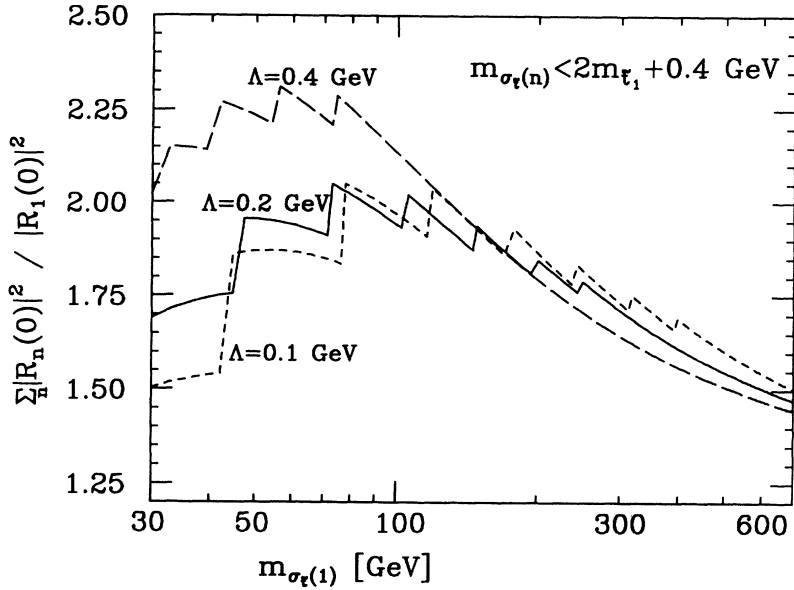
FIG. 9. Ratio $\sum_n |R_n(0)|^2/|R_1(0)|^2$, where n runs over all true top squarkonium bound states, defined by Eq. (17). This is a measure of the possible enhancement of the signal for top squarkonium production due to the production of excited states, as discussed in the text.

sume, rather conservatively, that the mass of the lightest top squark "meson" lies just 200 MeV above $m_{\tilde{t}_1}$; i.e., we treat the nth $\tilde{t}_1\tilde{t}_1^*$ state $\sigma_{\tilde{t}_1}(n)$ as a bound state if

$$m_{\sigma_{\tilde{t}}(n)} < 2m_{\tilde{t}_1} + 0.4 \text{ GeV} . \quad (17)$$

Of course, the wave function at the origin, and hence the production cross section, is smaller for excited states than for the ground state $[|R(0)|^2 \propto 1/n^2$ for a Coulomb potential]. Nevertheless, Fig. 9 shows that the enhancement of the signal due to the production of excited states can be quite substantial. In this figure we show $\sum_n |R_n(0)|^2/|R_1(0)|^2$, where the sum runs over all states that satisfy the condition (17), i.e., are true bound states. This ratio is equal to the enhancement of the signal due to the production of excited top squarkonium states if annihilation decays dominate the total $\sigma_{\tilde{t}_1}$ decay width and if the excited states themselves contribute to the signal in the same way as the ground state does.

This second requirement deserves a brief discussion. Since all excited states in the sum are S-wave states, expression (5) also describes their annihilation decays [with $R(0)$ replaced by $R_n(0)$]. The various top squarkonium states should lie close enough together that their $\gamma\gamma$ invariant-mass peaks will not be distinguished from each other by the detector, unless we have underestimated the resolution to be achieved by future experiments. Annihilation decays of the excited states will therefore contribute to the signal in the same way as for the ground state. However, these excited states have additional decay channels: They can decay into lower-lying top squarkonium states, plus a photon or a mesonic system with vanishing charge and strong isospin. Cascade decays of excited states into lower-lying S-wave states will also contribute to the signal if the lower-lying state decays into two photons, since the existence of additional very soft photons or mesons from the cascade will hardly be detectable at hadron colliders.

However, an excited state can also decay into a lower-lying state with *different* angular momentum, e.g., into a P-wave state. The relative branching ratios for annihilation decays of these higher-spin states can differ significantly from those of the S-wave states; Eq. (5) is no longer applicable here. In particular, P-wave states do not contribute to the signal at all (unless they in turn decay into another S-wave state), since they cannot decay into two photons. In order to estimate how much the higher S-wave states contribute to the signal, one would therefore have to follow all their decay chains; this necessitates a complete understanding of top squarkonium spectroscopy, which is well beyond the scope of this paper. We mention here that only a rather small fraction of $\Upsilon(2s)$ and $\Upsilon(3s)$ mesons decays into P-wave $b\bar{b}$ (χ_b) states which do not decay back into S-wave states [$\sim 13\%$ for $\Upsilon(2s)$ and $\sim 22\%$ for $\Upsilon(3s)$]. If this result carries over to the top squarkonium system, Fig. 9 should give a good estimate for the enhancement of the signal due to the production of excited states. Finally, there is a contribution to the signal from the direct production of states with $J\neq 0$ and their subsequent decay into S-wave states, but it should be quite small.[12]

In any case, in the absence of a more reliable treatment of the decays of excited squarkonium states we have con-

---

[12]In the most simple treatment of nonrelativistic bound states [35,36], the production cross section of higher-spin states is predicted to be small since it is proportional to the square of derivatives of the wave function at the origin, divided by additional powers of $m_{\tilde{t}_1}$. Recently, Bodwin et al. [55] have suggested that the production of P-wave quarkonia states might be enhanced by the presence of a sizable component of the wave function where the $Q\bar{Q}$ is in a color octet state. However, the same component would also suppress the branching ratio for P-wave states to decay into S-wave states, so that altogether the P-wave contribution to the $\gamma\gamma$ signal is still small.
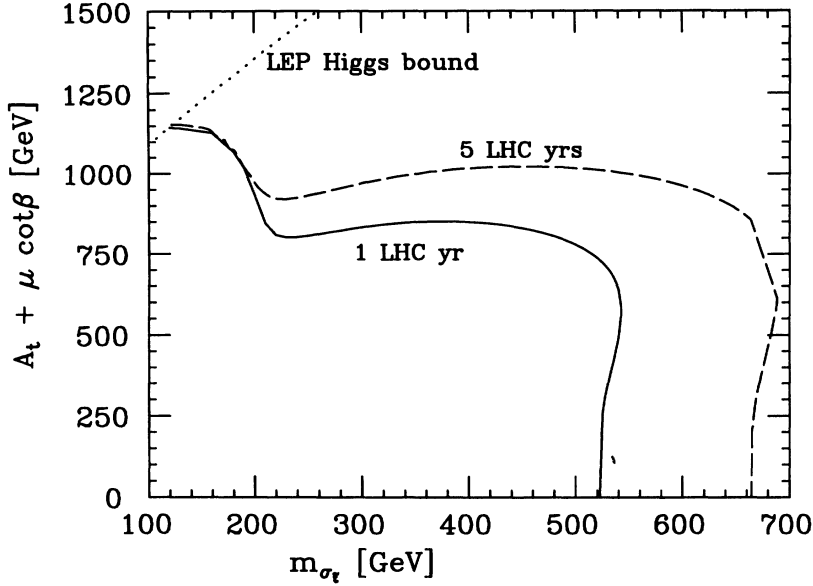
FIG. 10. Region in the plane spanned by $m_{\sigma_{\tilde{t}}}$ and $A_t + \mu \cot\beta$ that can be searched after 1 (solid curve) and 5 (dashed curve) years of running the LHC at full luminosity ($\mathcal{L} = 100$ fb^{-1} per year). The region in the top left corner is excluded by LEP searches for neutral Higgs bosons. The curves have been obtained for $m_t = 150$ GeV, $\tan\beta = 3$, $M_2 = 1.67 m_{\tilde{t}_1}$, $m_{\tilde{t}_L} = m_{\tilde{t}_R}$, $\mu = 750$ GeV, and $m_P = 2$ TeV, but depend little on these choices unless $m_{\sigma_{\tilde{t}}} \simeq m_P$, as discussed in the text.

servatively decided to only include the direct production of the lowest ($n = 1$) S-wave state in our estimates of signal cross sections.

We finally address the question of the $\sigma_{\tilde{t}_1}$ discovery potential of the LHC, using the $\gamma\gamma$ decay mode and our conservative estimate of the signal cross section. We have already stated repeatedly that $\sigma_{\tilde{t}_1}$ will be unobservable at hadron colliders and may indeed not form at all if the single top squark decay modes (4a) and (4b) are unsuppressed *or* $\sigma_{\tilde{t}_1}$ is very close in mass to one of the two scalar Higgs bosons of the MSSM; for the subsequent discussion, we therefore assume that this is not the case. We saw in Sec. II that the size of the $\gamma\gamma$ branching ratio is then almost uniquely determined by the partial width for the hh final state, the ratio of the gg and $\gamma\gamma$ partial widths being fixed by QCD. Moreover, we saw in Fig. 5 that, at least for parameters where $\Gamma(\sigma_{\tilde{t}_1} \to hh) \geq \Gamma(\sigma_{\tilde{t}_1} \to gg)$, the partial width for the hh final state is determined by the size of the LR element of the top squark mass matrix (1). Under the given assumptions, the detectability of the $\sigma_{\tilde{t}_1} \to \gamma\gamma$ signal at the LHC therefore basically depends on two parameters: the mass $m_{\sigma_{\tilde{t}}}$, which determines the total $\sigma_{\tilde{t}_1}$ production cross section, and $m_{LR}^2 = -m_t(A_t + \mu \cot\beta)$, which determines the size of the branching ratio of the $\gamma\gamma$ decay mode.

It can safely be assumed that the mass of the top quark will be known quite precisely before LHC experiments are ready to search for $\sigma_{\tilde{t}_1}$ production. In Fig. 10 we therefore show the region in the plane of $m_{\sigma_{\tilde{t}}}$ and $A_t + \mu \cot\beta$ that can be probed after 1 and 5 nominal LHC years ($\mathcal{L} = 100$ fb^{-1} per year). Here we have assumed $m_t = 150$ GeV and $\tan\beta = 3$, but this choice has little affect on the accessible region.[13]

---

[13]It does affect the size of the region in the top left corner where the LEP Higgs bound [45] is violated.

The general shape of the curves is easy to understand. At small $m_{\sigma_{\tilde{t}}}$ the hh mode is only open if $A_t + \mu \cot\beta$ is very large; note that radiative corrections reduce m_h if $A_t + \mu \cot\beta \gg m_{\tilde{t}_{L,R}}$ [33,34]. In this case the hh partial width is very large just beyond the threshold, as shown in Fig. 4, and the $\gamma\gamma$ signal remains unobservable even after a long running period. On the other hand, for larger $m_{\sigma_{\tilde{t}}}$ the hh channel is always open. We see that the curves for the maximal accessible $A_t + \mu \cot\beta$ become quite flat in this region. The reason is that increasing $m_{\sigma_{\tilde{t}}}$ decreases the total cross section for $\sigma_{\tilde{t}_1}$ production, but at the same time decreases the branching ratio for the hh mode if $A_t + \mu \cot\beta$ is kept fixed [see Eq. (8)]. Moreover, the minimal detectable signal cross section decreases with increasing $m_{\sigma_{\tilde{t}}}$, although more slowly than the total $\sigma_{\tilde{t}_1}$ production cross section does, as shown in Fig. 7. These effects tend to cancel each other, leading to the observed flattening of the curves for $m_{\sigma_{\tilde{t}}} \geq 220$ GeV. Eventually, however, increasing $m_{\sigma_{\tilde{t}}}$ reduces the hh partial width to a value below the gg partial width; decreasing it even further then has little effect on the signal, and the curves terminate rather abruptly. We finally note that the little bulge in the accessible regions at $A_t + \mu \cot\beta \simeq 600$ GeV occurs because for moderate values of m_{LR}^2 the hh partial width no longer grows monotonically with $A_t + \mu \cot\beta$, as we already saw in Fig. 5.

IV. SUMMARY AND CONCLUSIONS

In this paper we have studied the decays of S-wave $\tilde{t}_1 \tilde{t}_1^*$ bound states $\sigma_{\tilde{t}_1}$, as well as possible signals for their production at hadron colliders. We first argued in Sec. I that there are no strict bounds on $m_{\tilde{t}_1}$ which hold both for all $\tilde{t}_L$-$\tilde{t}_R$ mixing angles θ_t and all values of the LSP mass; even under relatively mild assumptions, a $\tilde{t}_1$ as light as 40 GeV is still allowed. This leaves a wide mass

region to be explored. We have seen that $\sigma_{\tilde{t}_1}$ production is only detectable at hadron colliders if $\tilde{t}_1$ has no unsuppressed tree-level two-body decays. Otherwise, single squark decays of $\sigma_{\tilde{t}_1}$ dominate over annihilation decays and top squarkonium production gives at best a small contribution to the signals for open top squark production.

The dominant annihilation decay modes of $\sigma_{\tilde{t}_1}$ are those into two gluons, two light scalar Higgs bosons h or a $t\bar{t}$ pair. Since the latter two decays involve electroweak rather than strong couplings, their partial widths have to be enhanced dynamically in order to be comparable to or larger than the one for the gg final state. In case of the $t\bar{t}$ mode, this can only happen if $m_{\sigma_{\tilde{t}}}$ is very close to the mass of the heavy scalar Higgs boson H, so that s-channel H exchange contributions become (almost) resonant. The hh partial width becomes large if the off-diagonal entry m_{LR}^2 of the top squark mass matrix is approximately as large as the diagonal entries of that matrix; in such a situation, mixing greatly reduces the mass of the lighter top squark eigenstate. Since the $h\tilde{t}_1\tilde{t}_1^*$ coupling increases with m_{LR}^2 while $m_{\tilde{t}_1}$ decreases, thereby further enhancing $\tilde{t}_1$ exchange diagrams, the hh partial width is very sensitive to m_{LR}^2, as illustrated in Fig. 5.

Unfortunately, we saw in Sec. III that none of these three potentially dominant final states leads to a readily detectable signal at hadron colliders. The most promising mode appears to be the $\sigma_{\tilde{t}_1} \to \gamma\gamma$ decay, which gives rise to a peak in the two-photon invariant-mass spectrum. We analyzed this signal in some detail, comparing it to the $\gamma\gamma$ continuum background. We found that existing Tevatron data might already begin to close the light top squark window left by LEP (where the $Z\tilde{t}_1\tilde{t}_1^*$ coupling is suppressed by mixing and the $\tilde{t}_1$-LSP mass difference is small). On the other hand, even for $\int \mathcal{L}\, dt = 1$ fb^{-1} the mass reach of the Tevatron only extends to $m_{\sigma_{\tilde{t}}} = 90$ GeV. Under favorable circumstances this mass reach can be extended to 500 (700) GeV after 1 (5) year(s) of operation at the LHC with full luminosity ($\mathcal{L} = 100$ fb^{-1} per year). Recall, however, that for $m_{\sigma_{\tilde{t}}} > 120$ GeV the hh decay mode of $\sigma_{\tilde{t}_1}$ might be open, which might greatly reduce the branching ratio for the $\gamma\gamma$ final state. More generally, LHC experiments will therefore only be able to probe a region in the $(m_{\sigma_{\tilde{t}}}, m_{LR}^2)$ plane (see Fig. 10).

We should remind the reader here that our calculation has considerable uncertainties, even beyond those intrinsic to any leading order QCD prediction for hadronic processes. On the one hand, we have ignored backgrounds from jets with very few charged particles, which could fake a single photon. This background is clearly detector dependent, but could potentially be sizable. On the other hand, our estimate for the signal rate is probably also too low, since we have ignored all contributions involving higher (excited) top squarkonium states. We saw in Fig. 9 that they might enhance the signal by as much as a factor of 2; however, a quantitative treatment of their contribution requires a detailed understanding of the entire top squarkonium system.

Once $\sigma_{\tilde{t}_1}$ production has been observed in the $\gamma\gamma$ channel, its mass will be known precisely. If 160 GeV $\leq m_{\sigma_{\tilde{t}}} \leq 300$ GeV, one might then be able to find evidence of $\sigma_{\tilde{t}_1}$ production also using the γZ and/or ZZ channel, where Z bosons decay into e^+e^- or $\mu^+\mu^-$ pairs; at least this task should be easier than searching for $\sigma_{\tilde{t}_1}$ production in these channels before $m_{\sigma_{\tilde{t}}}$ is known. Once the existence of $\sigma_{\tilde{t}_1}$ has been established, one might also try to look for its hh decay via the $\tau^+\tau^+\tau^-\tau^-$ final state. We saw that the cross section for this final state could be as large as 1 pb; the main problem here is to cleanly identify the τ leptons. Data taken at lower luminosity are probably more useful for this purpose, since the presence of multiple overlapping events will make τ identification even more difficult.

Once $m_{\sigma_{\tilde{t}}}$ is known, one can even contemplate studying it in some detail at a $\gamma\gamma$ collider. At least, in principle, such a device can be constructed [56] by backscattering laser photons off the electrons and positrons of an e^+e^- collider. The cross section for $\sigma_{\tilde{t}_1}$ production could be of the order of $(0.5$ pb$)/(m_{\sigma_{\tilde{t}}}/100$ GeV$)^3$. Moreover, by polarizing the incident photons one can greatly reduce backgrounds; e.g., $\gamma\gamma \to q\bar{q}$ production would be suppressed for light quarks if both photons have the same polarization, which might even allow one to detect $\sigma_{\tilde{t}_1} \to gg$ decays. The strong dependence of many partial widths on model parameters (see Figs. 2 and 4) makes their measurement either at a pp or a $\gamma\gamma$ collider very interesting and in particular offers one of the few possibilities to measure the size of the trilinear soft breaking parameter A_t.

Note that searches for top squarkonium production are in some sense complementary to searches for open top squark production. Top squarkonium states will be very difficult to detect and might not form at all if $\tilde{t}_1$ decays via two-body modes that are accessible at the tree level. On the other hand, open top squark production at hadron colliders will be difficult to detect either via its semileptonic decay or via a missing p_T signal unless the $\tilde{t}_1$-LSP mass difference is sizable. These two requirements are complementary because within the minimal SUSY model there is a strong correlation between the possibility of tree-level two-body decays of $\tilde{t}_1$ and a large $\tilde{t}_1$-LSP mass difference. This is obvious for the top squark $\to$ top + LSP decay, but also holds if the $\tilde{t}_1 \to b$ + chargino decay is allowed, at least in the case where the LSP (which we always assume to be the lightest neutralino) is dominantly a gaugino. A gauginolike LSP is favored dynamically in modes with radiative gauge symmetry breaking [10], as well as by cosmological considerations; unlike a Higgsino-like or mixed-state LSP, it can naturally explain the observed dark matter in the Universe [57,58].

We thus conclude that there should be a sizable $\tilde{t}_1$-LSP mass difference, which facilitates detection of open top squark production, if $\tilde{t}_1$ decays rapidly; if the $\tilde{t}_1$-LSP

mass difference is small, the light top squark is usually long lived and chances for top squarkonium production should be good. This complementarity is not perfect. On the one hand, the possibility of a large branching ratio of $\sigma_{\tilde{t}_1}$ into hh or, worse, $t\bar{t}$ final states means that we cannot derive a firm "no-loose" theorem for top squark searches at hadron or e^+e^- colliders. On the other hand, if $\tilde{t}_1$ is rather light, it might well be long lived even if the top squark–LSP mass difference is large, since for chargino masses below 100 GeV or so the rule of thumb that the chargino is twice as heavy as the LSP (for gauginolike LSP) need not apply. In such a scenario, *both* open top squark and top squarkonium production might be observable at hadron colliders, the former via the $\tilde{t}_1 \rightarrow c + \text{LSP}$ loop decay, the latter in the two-photon channel. Given the intimate connection between top squarks and the puzzle of electroweak symmetry breaking, in particular in models where this breaking occurs radiatively, experimental searches for any signal for scalar top production at present and future colliders are well worth the effort.

ACKNOWLEDGMENTS

APPENDIX

In this appendix we list the (squared) matrix elements for S-wave color singlet $\tilde{t}_1\tilde{t}_1^*$ pair annihilation into the two-body final states of Eqs. (7), as well as the widths for the single top squark decays of Eqs. (4a) and (4b). We do not include annihilation into two charginos, since this can only occur if the $\tilde{t}_1 \rightarrow \tilde{W}_1 + b$ decay is allowed, in which case it swamps all annihilation decays. Recall also that we assume $\tilde{t}_1$ to be the lightest strongly interacting supersymmetric particle.

We start with the annihilation decays. In the following expressions we have suppressed color indices; i.e., summation over colors has been performed. The resulting color factors are included explicitly. As already briefly noted in Sec. II, the color wave function in the initial state of the matrix element in Eq. (5) is given by $\frac{1}{3}\delta_{ab}$; after contraction with the color indices of the scattering amplitude, a sum over a and b has to be taken. Note that this is *not* normalized to unity, which explains the appearance of the color factor of 3 in Eq. (5); however, this normalization has the practical advantage that annihilation into two color singlet particles has color factor 1.

$gg, \gamma\gamma$ state

For an S-wave initial state, i.e., for $v \rightarrow 0$, these final states receive contributions only from four-point interactions [Fig. 1(c)]; the t- and u-channel $\tilde{t}_1$ exchange diagrams [Figs. 1(a) and 1(b)] vanish in this limit (for physical, i.e., transverse, gauge bosons). The squared gg amplitude can be written as

$$\sum_{\text{color,spins}} |\mathcal{M}(\tilde{t}_1\tilde{t}_1^* \rightarrow gg)|_{v=0}^2 = \tfrac{32}{9}g_s^4 . \tag{A1}$$

The squared amplitude for the $\gamma\gamma$ final state is given by

$$\sum_{\text{spins}} |\mathcal{M}(\tilde{t}s_1\tilde{t}_1^* \rightarrow \gamma\gamma)|_{v=0}^2 = 16q^4 e^4 , \tag{A2}$$

where $q = \tfrac{2}{3}$ is the charge of top squark.

W^+W^- final state

This final state receives contributions from diagrams with t-channel exchange of bottom squarks (only $\tilde{b}_L$ contributes if terms $\propto m_b$ are neglected), s-channel exchange of light $(h \equiv H_2)$, and heavy $(H \equiv H_1)$ neutral scalar Higgs bosons, and also from the four-point interaction of two top squarks and two W bosons. The s-channel exchange of the Z boson does not contribute to the S-wave amplitude. Here we list the amplitude for specific helicities $\lambda, \bar{\lambda}$ of the W bosons; $\lambda, \bar{\lambda}$ can take the values $0, \pm 1$:

$$\mathcal{M}^{\lambda\bar{\lambda}}(\tilde{t}_1\tilde{t}_1^* \rightarrow W^+W^-)$$

$$= \gamma_W^{2-|\lambda|-|\bar{\lambda}|}(\delta_{\lambda 0}\delta_{\bar{\lambda}0}\beta_W^2 + (-1)^\lambda\delta_{\lambda\bar{\lambda}})$$

$$\times \left[\frac{1}{2}g^2\cos^2\theta_t - \sum_i \frac{g_{H_i WW}c_{\tilde{t}_1}^{(i)}}{4m_{\tilde{t}_1}^2 - m_{H_i}^2} \right]$$

$$- 2\beta_W^2\gamma_W^2\delta_{\lambda 0}\delta_{\bar{\lambda}0}g^2\cos^2\theta_t \frac{m_{\tilde{t}_1}^2}{m_{\tilde{t}_1}^2 + m_{\tilde{b}_L}^2 - m_W^2} . \tag{A3}$$

The other combinations of helicities do not contribute; this is easily understood from spin conservation. In Eq. (A3) we have introduced $\gamma_W = m_{\tilde{t}_1}/m_W$ and $\beta_W = \sqrt{1 - (m_W/m_{\tilde{t}_1})^2}$; γ_W appears in the polarization vector of longitudinal gauge bosons $(\lambda = 0)$. We have included mixing between SU(2) doublet and singlet tops squarks $(\tilde{t}_L, \tilde{t}_R)$, defined as in Eq. (2) of the main text; however, we ignored sbottom mixing. The $g_{H_i WW}$ are the Higgs W^+W^- couplings [32]:

$$g_{H_1 WW} = gm_W\cos(\beta - \alpha), \quad g_{H_2 WW} = gm_W\sin(\beta - \alpha) . \tag{A4}$$

The Higgs $\tilde{t}_1\tilde{t}_1^*$ couplings $c_{\tilde{t}_1}^{(i)}$ are defined in Eqs. (A3)–(A5) of Ref. [41]; we list them here for completeness:

$$c_{\tilde{t}_1}^{(i)} = \frac{gm_Z}{\cos\theta_W} s^{(i)}(\tfrac{1}{2}\cos^2\theta_t - \tfrac{2}{3}\sin^2\theta_W \cos2\theta_t)$$

$$+ \frac{gm_t^2}{m_W}r_u^{(i)} - \frac{gm_t\sin2\theta_t}{2m_W}(A_t r_u^{(i)} + \mu r_u'^{(i)}),\qquad \text{(A5)}$$

where

$$s^{(1)} = -\cos(\alpha+\beta),\quad s^{(2)} = \sin(\alpha+\beta),$$

$$r_u^{(1)} = -\frac{\sin\alpha}{\sin\beta},\quad r_u^{(2)} = -\frac{\cos\alpha}{\sin\beta},\qquad \text{(A6)}$$

$$r_u'^{(1)} = -\frac{\cos\alpha}{\sin\beta},\quad r_u'^{(2)} = \frac{\sin\alpha}{\sin\beta}.$$

Here $\tan\beta$ is the ratio of vacuum expectation values introduced in Sec. II and α is the mixing angle of the neutral scalar Higgs bosons [32]. Note that $r_u^{(2)}\rightarrow1$ and $r_u'^{(2)}\rightarrow\cot\beta$ if the pseudoscalar Higgs boson is much heavier than m_Z; the last term in Eq. (A5) is thus proportional to the off-diagonal entry of the top squark mass matrix in this limit, as emphasized in the text.

ZZ final state

The contributing Feynmann diagrams are similar to those for the W^+W^- final state, except now the t-channel exchanges proceed through $\tilde{t}_{1,2}$, and crossed (u-channel) diagrams have to be added since the Z bosons do not carry a charge. We find

$$\mathcal{M}^{\lambda\bar{\lambda}}(\tilde{t}_1\tilde{t}_1^* \rightarrow ZZ)_{v=0} = -\gamma_Z^{2-|\lambda|-|\bar{\lambda}|}(\delta_{\lambda0}\delta_{\bar{\lambda}0}\beta_Z^2 + (-)^\lambda \delta_{\lambda\bar{\lambda}})$$

$$\times \frac{1}{\cos^2\theta_W}\left[2g^2[(\tfrac{1}{4}-\tfrac{2}{3}\sin^2\theta_W)\cos^2\theta_t + \tfrac{4}{9}\sin^4\theta_W] - \sum_i \frac{g_{H_i WW}c_{\tilde{t}_1}^{(i)}}{4m_{\tilde{t}_1}^2 - m_{H_i}^2}\right]$$

$$+ \frac{2g^2 m_{\tilde{t}_1}^2}{\cos^2\theta_W}\beta_Z^2\gamma_Z^2\delta_{\lambda0}\delta_{\bar{\lambda}0}\left[\frac{(\cos^2\theta_t - \tfrac{4}{3}\sin^2\theta_W)^2}{2m_{\tilde{t}_1}^2 - m_Z^2} + \frac{\cos^2\theta_t \sin^2\theta_t}{m_{\tilde{t}_1}^2 + m_{\tilde{t}_2}^2 - m_Z^2}\right],\qquad \text{(A7)}$$

where $\gamma_Z = m_{\tilde{t}_1}/m_Z$ and $\beta_Z = \sqrt{1-(m_Z/m_{\tilde{t}_1})^2}$.

$Z\gamma$ final state

Since the photon does not have longitudinal polarization states, the t- and u-channel exchange of $\tilde{t}_1$ again disappears in the $v\rightarrow0$ limit. Furthermore, only $\lambda_Z = \lambda_\gamma = \pm1$ states are allowed. After summing over the final state polarization, we get

$$\sum_{\text{spin}} |\mathcal{M}(\tilde{t}_1\tilde{t}_1^* \rightarrow Z\gamma)|_{v=0}^2 = \frac{8q^2 e^2 g^2}{\cos^2\theta_W}(\tfrac{1}{2}\cos^2\theta_t - \tfrac{2}{3}\sin^2\theta_W)^2.\qquad \text{(A8)}$$

hh final state

Here all four classes of diagrams depicted in Fig. 1 contribute:

$$\mathcal{M}(\tilde{t}_1\tilde{t}_1^* \rightarrow hh)|_{v=0} = \left\{\frac{2(c_{\tilde{t}_1}^{(2)})^2}{2m_{\tilde{t}_1}^2 - m_{H_2}^2} + \frac{2(c_{\tilde{t}_1\tilde{t}_2}^{(2)})^2}{m_{\tilde{t}_1}^2 + m_{\tilde{t}_2}^2 - m_{H_2}^2} + c_{11}^{22}\right.$$

$$+ \frac{c_{\tilde{t}_1}^{(1)}}{4m_{\tilde{t}_1}^2 - m_{H_1}^2}\frac{gm_Z}{2\cos\theta_W}[2\sin2\alpha\sin(\beta+\alpha) - \cos(\beta+\alpha)\cos2\alpha]$$

$$\left. + \frac{c_{\tilde{t}_1}^{(2)}}{4m_{\tilde{t}_1}^2 - m_{H_2}^2}\frac{3gm_Z}{2\cos\theta_W}\cos2\alpha\sin(\beta+\alpha)\right\}.\qquad \text{(A9)}$$

Here $c_{\tilde{t}_1\tilde{t}_2}^{(2)}$ and c_{11}^{22} are the $\tilde{t}_1$-$\tilde{t}_2$-h and $\tilde{t}_1$-$\tilde{t}_1$-h-h couplings, respectively; they can be expressed as

$$c_{\tilde{t}_1\tilde{t}_2}^{(2)} = g\frac{m_Z\sin(\alpha+\beta)}{\cos\theta_W}\sin2\theta_t(\tfrac{2}{3}\sin^2\theta_W - \tfrac{1}{4}) + \frac{gm_t}{2m_W\sin\beta}(A_t\cos\alpha - \mu\sin\alpha)\cos2\theta_t,\qquad \text{(A10a)}$$

$$c_{11}^{22} = \frac{g^2}{2} \left[\frac{\cos 2\alpha}{\cos^2 \theta_W} (\tfrac{1}{2} \cos^2 \theta_t - \tfrac{2}{3} \sin^2 \theta_W \cos 2\theta_t) - \frac{m_t^2}{m_W^2} \frac{\cos^2 \alpha}{\sin^2 \beta} \right] . \tag{A10b}$$

$\tilde{Z}_i \tilde{Z}_j$ final state

This process proceeds by t- and u-channel exchange of a top quark and s-channel exchange of Higgs bosons. In our convention neutralino eigenstates are obtained by diagonalizing the neutralino mass matrix by a real orthogonal matrix; thus, the mass eigenvalue of a neutralino can be either positive or negative. Defining h and $\bar{h}$ to be the helicities of the two neutralinos $(h, \bar{h} = \pm \tfrac{1}{2})$, we have

$$\mathcal{M}(\tilde{t}_1 \tilde{t}_1^* \rightarrow \tilde{Z}_i \tilde{Z}_j) = \delta_{h\bar{h}} \sqrt{4 m_{\tilde{t}_1}^2 - (m_{\tilde{Z}_i} + m_{\tilde{Z}_j})^2}$$

$$\times \left\{ \frac{2 m_t (a_i a_j - b_i b_j) + (m_{\tilde{Z}_i} + m_{\tilde{Z}_j})(a_i a_j + b_i b_j)}{\tfrac{1}{2}(m_{\tilde{Z}_1}^2 + m_{\tilde{Z}_j}^2) - m_{\tilde{t}_1}^2 - m_t^2} \right.$$

$$\left. + g \left[\frac{c_{\tilde{t}_1}^{(1)} (\sin \alpha S_{ij}'' - \cos \alpha Q_{ij}'')}{4 m_{\tilde{t}_1}^2 - m_{H_1}^2} + \frac{c_{\tilde{t}_1}^{(2)} (\sin \alpha Q_{ij}'' + \cos S_{ij}'')}{4 m_{\tilde{t}_1}^2 - m_{H_2}^2} \right] \right\} . \tag{A11}$$

Here a_i and b_i are scalar and pseudoscalar top-squark–top-quark–neutralino couplings; explicit expressions are given in Eqs. (3), (8), and (9) of Ref. [41]. Q_{ij}'' and S_{ij}'' are Higgs-boson–neutralino couplings defined in Ref. [32]; recall that they are real in our notation.

$b\bar{b}$ final state

This process proceeds via the t-channel exchange of charginos $(\tilde{W}_1, \tilde{W}_2)$ as well as s-channel exchange of Higgs bosons:

$$\mathcal{M}(\tilde{t}_1 \tilde{t}_1^* \rightarrow b\bar{b}) = -\delta_{h\bar{h}} 2\sqrt{3} \sqrt{m_{\tilde{t}_1}^2 - m_b^2}$$

$$\times \left\{ \sum_{i=1}^{2} \frac{1}{3} \frac{m_{\tilde{W}_1}(c_i^2 - d_i^2) + m_b(c_i^2 + d_i^2)}{m_b^2 - m_{\tilde{t}_1}^2 - m_{\tilde{W}_i}^2} + \frac{g m_b}{2 m_W \cos \beta} \left[-\frac{c_{\tilde{t}_1}^{(1)} \cos \alpha}{4 m_{\tilde{t}_1}^2 - m_{H_1}^2} + \frac{c_{\tilde{t}_1}^{(2)} \sin \alpha}{4 m_{\tilde{t}_1}^2 - m_{H_2}^2} \right] \right\} . \tag{A12}$$

Here h and $\bar{h}$ are again the final state helicities, and c_i and d_i are scalar and pseudoscalar top-squark–bottom–chargino couplings defined as

$$\mathcal{L}_{\tilde{t}_1 \tilde{W}_1 b} = \bar{b}(c_i + d_i \gamma_5) \tilde{W}_i \tilde{t}_1 + \text{H.c.} , \tag{A13a}$$

$$c_i = -\frac{g}{2} V_{i1} \cos \theta_t + \frac{g m_b U_{i2}}{2\sqrt{2} m_W \cos \beta} \cos \theta_t + \frac{g m_t V_{i2}}{2\sqrt{2} m_W \sin \beta} \sin \theta_t , \tag{A13b}$$

$$d_i = -\frac{g}{2} V_{i1} \cos \theta_t - \frac{g m_b U_{i2}}{2\sqrt{2} m_W \cos \beta} \cos \theta_t + \frac{g m_t V_{i2}}{2\sqrt{2} m_W \sin \beta} \sin \theta_t . \tag{A13c}$$

U_{ij} and V_{ij} are [32] the matrices that diagonalize the chargino mass matrix. We use the same conventions as in Eqs. (A6)–(A8) of Ref. [58]; in particular, $m_{\tilde{W}_{1,2}}$ can have either sign. Note that $c_i^2 - d_i^2$ is proportional to m_b; hence, the whole cross section is suppressed by the square of the bottom quark mass. This decay mode therefore turns out to be negligible for the whole parameter space of our interests, unless it is "accidentally" enhanced by an s-channel (h or H) pole. The factor of $\tfrac{1}{3}$ for the $\tilde{W}_i$ exchange term is a color factor necessary for t-channel color singlet exchange. We have included an overall color factor of $\sqrt{3}$, which strictly speaking only occurs after the (incoherent) summation over the final state color indices.

$t\bar{t}$ final state

This process proceeds t-channel exchange of neutralinos and gluinos $(\tilde{g})$ and s-channel exchange of scalar Higgs bosons:

$$\mathcal{M}(\tilde{t}_1 \tilde{t}_1^* \to t\bar{t})|_{v=0} = -2\delta_{h\bar{h}}\sqrt{3}\sqrt{m_{\tilde{t}_1}^2 - m_t^2}$$

$$\times \left\{ \frac{1}{3} \sum_{i=1}^{4} \frac{m_{\tilde{Z}_i}(a_i^2 - b_i^2) + m_t(a_i^2 + b_i^2)}{m_t^2 - m_{\tilde{t}_1}^2 - m_{\tilde{Z}_i}^2} + \frac{4}{9} \frac{m_{\tilde{g}}(a_{\tilde{g}}^2 - b_{\tilde{g}}^2) + m_t(a_{\tilde{g}}^2 + b_{\tilde{g}}^2)}{m_t^2 - m_{\tilde{t}_1}^2 - m_{\tilde{g}}^2} \right.$$

$$\left. - \frac{gm_t}{2m_W \sin\beta} \left[\frac{c_{\tilde{t}_1}^{(1)} \sin\alpha}{4m_{\tilde{t}_1}^2 - m_{H_1}^2} + \frac{c_{\tilde{t}_1}^{(2)} \cos\alpha}{4m_{\tilde{t}_1}^2 - m_{H_2}^2} \right] \right\} . \tag{A14}$$

The couplings a_i, b_i have already occurred in Eq. (A11) above; $a_{\tilde{g}}, b_{\tilde{g}}$ are the corresponding gluino–top-squark–top-quark couplings:

$$a_{\tilde{g}}^2 + b_{\tilde{g}}^2 = g_3^2, \quad a_{\tilde{g}}^2 - b_{\tilde{g}}^2 = -g_3^2 \sin2\theta_t . \tag{A15}$$

Here again the $\tilde{Z}_i$ exchange term receives a color factor of $\frac{1}{3}$, while the $\tilde{g}$ exchange contribution comes with a factor of $\frac{4}{9}$ for color octet exchange. Note that we have again included an overall factor of $\sqrt{3}$, which properly only appears in the squared amplitude after summation over the $t\bar{t}$ color states.

Single top squark decays: $\tilde{t}_1 \to \tilde{W}_i + b, \tilde{Z}_j + t$

If the top squark mass is larger than $m_{\tilde{W}_1} + m_b$ or $m_{\tilde{Z}_1} + m_t$, single top squark decays dominate and the pair annihilation modes described above all have a very small branching ratio. The decay width into $b + \tilde{W}_i$ is given by

$$\Gamma(\tilde{t}_1 \to b\tilde{W}_i^+) = \frac{|\mathcal{M}|^2}{16\pi m_{\tilde{t}_1}} \left[\left[1 - \frac{m_b^2 + m_{\tilde{W}_i}^2}{m_{\tilde{t}_1}^2} \right]^2 - \frac{4m_b^2 m_{\tilde{W}_i}^2}{m_{\tilde{t}_1}^4} \right]^{1/2} , \tag{A16}$$

where

$$\sum_{\text{spin}} |\mathcal{M}|^2 = 2c_i^2[m_{\tilde{t}_1}^2 - (m_b + m_{\tilde{W}_i})^2] + 2d_i^2[m_{\tilde{t}_1}^2 - (m_b - m_{\tilde{W}_i})^2] . \tag{A17}$$

The couplings c_i and d_i have been defined in Eq. (A13). Equations (A16) and (A17) also describe the decay width for $\tilde{t}_1 \to \tilde{Z}_j + t$, with the following substitutions: $m_b \to m_t$, $m_{\tilde{W}_i} \to m_{\tilde{Z}_j}$, $c_i \to a_j$, and $d_i \to b_j$; the $t\tilde{t}_1\tilde{Z}_j$ couplings a_j and b_j have already been introduced in Eq. (A11).

[1] S. L. Glashow, Nucl. Phys. B22, 579 (1961); S. Weinberg, Phys. Rev. Lett. 19, 1264 (1967); A. Salam, in *Elementary Particle Theory: Relativistic Groups and Analyticity (Nobel Symposium No. 8)*, edited by N. Svartholm (Almqvist and Wiksell, Stockholm, 1969), p. 367.

[2] L. Susskind, Phys. Rev. D 20, 2619 (1980); G. 't Hooft, in *Recent Developments in Gauge Theories*, Proceedings of the Cargèse Summer Institute, Cargèse, France, 1979, edited by G. 't Hooft *et al.*, NATO Advanced Study Institutes Series B: Physics Vol. 59 (Plenum, New York, 1980), p. 135; M. Veltman, Acta Phys. Pol. B 12, 437 (1981).

[3] E. Witten, Nucl. Phys. B188, 513 (1981); N. Sakai, Z. Phys. C 11, 153 (1981); S. Dimopoulos and H. Georgi, Nucl. Phys. B193, 150 (1981).

[4] For reviews, see H. E. Haber and G. L. Kane, Phys. Rep. 117, 75 (1985); H. P. Nilles, *ibid.* 110, 1 (1984); P. Nath, A. Arnowitt, and A. Chamseddine, *Applied N = 1 Supergravity*, ITCP Series in Theoretical Physics (World Scientific, Singapore, 1984); X. Tata, in *The Standard Model and Beyond*, edited by J. E. Kim (World Scientific, Singapore, 1991), p. 304.

[5] CDF Collaboration, F. Abe *et al.*, Phys. Rev. Lett. 69,

3439 (1992).

[6] For a review, see ALEPH Collaboration, D. Decamp *et al.*, Phys. Rep. 216, 253 (1992).

[7] Recent examples are H. Baer, A. Bartl, D. Karatas, W. Majerotto, and X. Tata, Int. J. Mod. Phys. A 4, 4111 (1989); H. Baer, X. Tata, and J. Woodside, Phys. Rev. D 42, 1568 (1990); 45, 142 (1992); R. M. Barnett, J. F. Gunion, and H. E. Haber, Phys. Lett. B 315, 349 (1993).

[8] U. Amaldi, W. de Boer, and H. Fürstenau, Phys. Lett. B 260, 447 (1991); P. Langacker and M. Luo, Phys. Rev. D 44, 817 (1991); J. Ellis, S. Kelley, and D. V. Nanopoulos, Phys. Lett. B 260, 131 (1991).

[9] G. G. Ross and R. G. Roberts, Nucl. Phys. B377, 571 (1991); P. Langacker and N. Polonsky, Phys. Rev. D 47, 4028 (1993); V. Barger, M. S. Berger, and P. Ohmann, *ibid.* 47, 1093 (1993); M. Carena, S. Pokorski, and C. E. M. Wagner, Nucl. Phys. B406, 59 (1993); Y. Yamada, Z. Phys. C 60, 83 (1993); A. E. Faraggi and B. Grinstein, Report No. SSCL-PREPRINT-496 (unpublished).

[10] K. Inoue, A. Kakuto, H. Komatsu, and S. Takeshita, Prog. Theor. Phys. 68, 927 (1982); 71, 413 (1984); L. E. Ibáñez and G. G. Ross, Phys. Lett. 110B, 215 (1982); L. E.

Ibáñez, *ibid.* **118B**, 73 (1982); J. Ellis, D. V. Nanopoulos, and K. Tamvakis, *ibid.* **121B**, 123 (1983); L. Alvarez-Gaumé, J. Polchinski, and M. Wise, Nucl. Phys. **B221**, 495 (1983); L. E. Ibáñez and C. Lopez, *ibid.* **B233**, 511 (1984); C. Kounnas, A. B. Lahanas, D. V. Nanopoulos, and M. Quirós, *ibid.* **B236**, 438 (1984); A. Bouquet, J. Kaplan, and C. A. Savoy, *ibid.* **B262**, 299 (1985); G. F. Giudice and G. Ridolfi, Z. Phys. C **41**, 447 (1988); R. Barbieri and G. F. Giudice, Nucl. Phys. **B306**, 63 (1988); W. Majerotto and B. Mösslacher, Z. Phys. C **48**, 273 (1990); Ross and Roberts [9]; S. Kelley, J. L. Lopez, D. V. Nanopoulos, H. Pois, and K. Yuan, Nucl. Phys. **B398**, 3 (1993); P. Nath and A. Arnowitt, Phys. Rev. Lett. **70**, 3696 (1993); B. de Carlos and J. A. Casas, Phys. Lett. B **309**, 320 (1993); M. Olechowski and S. Pokorski, Nucl. Phys. **B404**, 590 (1993); D. J. Castano, E. J. Piard, and P. Ramond, Phys. Rev. D (to be published); V. Barger, M. S. Berger, and P. Ohmann, *ibid.* (to be published).

[11] J. Ellis and S. Rudaz, Phys. Lett. **128B**, 248 (1983).

[12] M. Drees and M. M. Nojiri, Nucl. Phys. **B369**, 54 (1992).

[13] T. Kon and T. Nonaka, Phys. Lett. B **319**, 355 (1993).

[14] H. Baer, M. Drees, R. Godbole, J. F. Gunion, and X. Tata, Phys. Rev. D **44**, 725 (1991).

[15] M. Drees and K.-I. Hikasa, Phys. Lett. B **252**, 127 (1990).

[16] TOPAZ Collaboration, R. Enomoto *et al.*, Report No. KEK-PREPRINT-93-107 (unpublished).

[17] R. Enomoto, talk presented at the 2nd Workshop on TRISTAN Physics at High Luminosities, KEK, Tsukuba, Japan, 1993 (unpublished).

[18] Y. Okada, Phys. Lett. B **315**, 119 (1993).

[19] M. Drees, M. Krämer, J. Zunft, and P. Zerwas, Phys. Lett. B **252**, 371 (1993).

[20] S. Iwata, talk presented on the 9th Topical Workshop on $p\bar{p}$ Collider Physics, Tsukuba, 1993 (unpublished); J. Shirai, talk presented at the 2nd Workshop on TRISTAN Physics at High Luminosities [17].

[21] M. Drees, K. Hagiwara, and A. Yamada, Phys. Rev. D **45**, 1725 (1992), and references therein; for a recent assessment, see G. Altarelli, R. Barbieri, and F. Caravaglios, Phys. Lett. B **314**, 357 (1993).

[22] LEP Collaboration and LEP Electroweak Working Group, presented at the European Conference on High Energy Physics, Marseille, France 1993 (unpublished).

[23] CDF Collaboration, F. Abe *et al.*, Phys. Rev. D **45**, 3921 (1992); Fermilab Report No. CONF-93-212-E (unpublished); D0 Collaboration, R. Raja talk presented at the 7th Rencontres de Physique de la Vallée d'Aoste, La Thuile, Italy, 1993, Fermilab Report No. CONF-93-143-E (unpublished).

[24] S. Bertolini, F. Borzumati, A. Masiero, and G. Ridolfi, Nucl. Phys. **B353**, 591 (1991); F. Borzumati, DESY No. Report 93-090 (unpublished).

[25] CLEO Collaboration, E. Thorndike *et al.*, Phys. Rev. Lett. **71**, 674 (1993).

[26] T. K. Hemmick *et al.*, Phys. Rev. D **41**, 2074 (1991).

[27] K.-I. Hikasa and M. Kobayashi, Phys. Rev. D **36**, 724 (1987).

[28] M. J. Herrero, A. Méndez, and T. G. Rizzo, Phys. Lett. B **200**, 205 (1988).

[29] V. Barger and W.-Y. Keung, Phys. Lett. B **211**, 355 (1988).

[30] H. Inazawa and T. Morii, Phys. Rev. Lett. **70**, 2992 (1993).

[31] M. Drees and M. M. Nojiri, Phys. Rev. Lett. (to be published).

[32] J. F. Gunion and H. E. Haber, Nucl. Phys. **B272**, 1 (1986).

[33] Y. Okada, M. Yamaguchi, and T. Yanagida, Prog. Theor. Phys. **85**, 1 (1991); Phys. Lett. B **262**, 54 (1991); H. E. Haber and R. Hempfling, Phys. Rev. Lett. **66**, 1815 (1991); R. Barbieri, M. Frigeni, and F. Caravaglios, Phys. Lett. B **258**, 395 (1991); A. Yamada, *ibid.* **263**, 233 (1991).

[34] J. Ellis, G. Ridolfi, and F. Zwirner, Phys. Lett. B **257**, 83 (1991); **262**, 477 (1991); M. Drees and M. M. Nojiri, Phys. Rev. D **45**, 2482 (1992); A. Brignole, Phys. Lett. B **281**, 284 (1992); J. Kodaira, Y. Yasui, and K. Sasaki, Hiroshima University Report No. HUPD-9316 (unpublished).

[35] J. H. Kühn, J. Kaplan, and E. G. Safiani, Nucl. Phys. **B157**, 125 (1979); B. Guberina, J. H. Kühn, R. Peccei, and R. Rückl, *ibid.* **B174**, 317 (1980).

[36] V. Barger, E. W. N. Glover, K.-I. Hikasa, W.-Y. Keung, M. G. Olsson, C. J. Suchyta, and X. R. Tata, Phys. Rev. D **35**, 3366 (1987).

[37] K. Hagiwara, K. Kato, A. D. Martin, and C.-K. Ng, Nucl. Phys. **B344**, 1 (1990).

[38] V. S. Fadin and V. A. Khoze, Pis'ma Zh. Eksp. Teor. Fiz. **46**, 417 (1987) [JETP Lett. **46**, 525 (1987)]; M. J. Strassler and M. E. Peskin, Phys. Rev. D **43**, 1500 (1991); Y. Sumino, K. Fujii, K. Hagiwara, H. Murayama, and C.-K. Ng, *ibid.* **47**, 56 (1992).

[39] I. I. Bigi, V. S. Fadin, and V. Khoze, Nucl. Phys. **B377**, 461 (1992).

[40] J. Ellis, M. K. Gaillard, D. V. Nanopoulos, and C. T. Sachrajda, Phys. Lett. **83B**, 339 (1979); M. Drees and K.-I. Hikasa, Phys. Rev. D **41**, 1547 (1990).

[41] M. Drees and M. M. Nojiri, Phys. Rev. D **48**, 3483 (1993).

[42] B. W. Lee, C. Quigg, and H. Thacker, Phys. Rev. D **16**, 1519 (1977); M. S. Chanowitz and M. K. Gaillard, Nucl. Phys. **B261**, 379 (1985); H. Veltman, Phys. Rev. D **41**, 2294 (1990).

[43] J. F. Owens, Phys. Lett. B **266**, 126 (1991).

[44] V. Barger and R. J. N. Phillips, *Collider Physics* (Addison-Wesley, Reading, MA, 1987).

[45] ALEPH Collaboration, D. Decamp *et al.*, Phys. Lett. B **265**, 475 (1991); L3 Collaboration, B. Adeva *et al.*, *ibid.* **283**, 454 (1992); DELPHI Collaboration, P. Abreau *et al.*, Nucl. Phys. **B373**, 3 (1992).

[46] A. Djouadi, J. Kalinowski, and P. M. Zerwas, Z. Phys. C **57**, 569 (1993).

[47] R. S. Fletcher, F. Halzen, and C. S. Kim, Phys. Lett. B **209**, 351 (1988).

[48] J. Ohnemus, Phys. Rev. D **47**, 336 (1992).

[49] D. A. Dicus and S. S. D. Willenbrock, Phys. Rev. D **37**, 1801 (1988); H. A. Baer and J. F. Owens, Phys. Lett. B **205**, 377 (1988).

[50] B. Bailey, J. Ohnemus, and J. F. Owens, Phys. Rev. D **46**, 2018 (1992); B. Bailey and J. F. Owens, *ibid.* **47**, 2735 (1993).

[51] H. Baer, M. Bisset, C. Kao, and X. Tata, Phys. Rev. D **46**, 1067 (1992).

[52] CDF Collaboration, F. Abe *et al.*, Phys. Rev. Lett. **70**, 2232 (1993).

[53] J. H. Kühn and E. Mirkes, Phys. Rev. D **48**, 179 (1993).

[54] J. G. Morfin and W.-K. Tung, Z. Phys. C **52**, 13 (1991).

[55] G. T. Bodwin, E. Braaten, and G. P. Lepage, Phys. Rev. D **46**, 1914 (1992).

[56] I. F. Ginzburg, G. L. Kotkin, V. G. Serbo, and V. I. Telnov, Nucl. Instrum. Methods **205**, 219 (1983); **219**, 5 (1984).

[57] Some recent papers are K. Griest, M. Kamionkowski, and M. Turner, Phys. Rev. D **41**, 3565 (1990); K. Olive and M.

Srednicki, Nucl. Phys. **B355**, 208 (1991); J. Ellis and L. Roszkowski, Phys. Lett. B **283**, 252 (1992). The importance for "coannihilation" of the LSP with the next-to-lightest sparticle for a Higgsino-like LSP has been em-phasized by S. Mizuta and M. Yamaguchi, *ibid.* **298**, 120 (1993).

[58] M. Drees and M. M. Nojiri, Phys. Rev. D **47**, 376 (1993).